

SLOWLY MODULATED TWO-PULSE SOLUTIONS IN THE GRAY–SCOTT MODEL II: GEOMETRIC THEORY, BIFURCATIONS, AND SPLITTING DYNAMICS*

ARJEN DOELMAN[†], WIKTOR ECKHAUS[‡], AND TASSO J. KAPER[§]

With great sadness, we note the passing away of our mentor and colleague Wiktor

Abstract. In this second paper, we develop a geometrical method to systematically study the singular perturbed problem associated to slowly modulated two-pulse solutions. It enables one to see that the characteristics of these solutions are strongly determined by the flow on a slow manifold and, hence, also to identify the saddle-node bifurcations and bifurcations to classical traveling waves in which the solutions constructed in part I are created and annihilated. Moreover, we determine the geometric origin of the critical maximum wave speeds discovered in part I. In this paper, we also study the central role of the slowly varying inhibitor component of the two-pulse solutions in the pulse-splitting bifurcations. Finally, the validity of the quasi-stationary approximation is established here, and we relate the results of both parts of this work to the literature on self-replication.

Key words. reaction-diffusion equations, modulated traveling waves, singular perturbation theory, self-replicating patterns

AMS subject classifications. 35K57, 35B25, 35B32, 35B40, 34C37, 92E20

PII. S0036139900372429

1. Introduction. In this paper, we continue our study of slowly modulated two-pulse solutions in the one-dimensional Gray–Scott model:

$$(1.1) \quad \frac{\partial U}{\partial t} = \frac{\partial^2 U}{\partial x^2} - UV^2 + A(1 - U), \quad \frac{\partial V}{\partial t} = D \frac{\partial^2 V}{\partial x^2} + UV^2 - BV,$$

where A, B , and D are positive parameters. See [9, 17, 18, 2, 1] for more background.

The slowly modulated two-pulse solutions are constructed by a so-called quasi-stationary approach in part I [1]. The key ingredients of our analysis of these solutions are (i) the observation that the “fast” V -components are exponentially small except for asymptotically small intervals in which V has an asymptotically large “pulse,” while the “slow” U -components are not localized (see Figure 1 in part I); (ii) the decomposition of the pair of traveling pulses into a part traveling to the right (on $[0, \infty)$) and a part traveling to the left (on $(-\infty, 0]$) (see Figure 1 in part I); (iii) the introduction of a traveling coordinate ξ in which the speed $c = c(t)$ is allowed to vary slowly in time; (iv) the assumption that the explicit time derivative terms $\partial U/\partial t$ and $\partial V/\partial t$ are small and hence can be neglected to leading order; and (v) the application of boundary conditions at the “overlap point” $x = 0$ and as $\xi \rightarrow \pm\infty$. As in part I,

*Received by the editors April 26, 1999; accepted for publication (in revised form) April 10, 2000; published electronically April 24, 2001.

<http://www.siam.org/journals/siap/61-6/37242.html>

[†]Korteweg-deVries Instituut, Universiteit van Amsterdam, Plantage Muidergracht 24, 1018TV Amsterdam, The Netherlands (doelman@wins.uva.nl). The research of this author was supported by the Organization for Scientific Research (NWO).

[‡]The author is deceased. Former address: Mathematisch Instituut, Universiteit Utrecht, P.O. Box 80.010, 3508TA Utrecht, The Netherlands.

[§]Department of Mathematics & Center for BioDynamics, Boston University, 111 Cummington Street, Boston, MA 02215 (tasso@math.bu.edu). The research of this author was supported by the National Science Foundation through CAREER grant DMS-9624471 and a Sloan Research Fellowship (1995–1998).

we focus on the symmetric case, in which the left and right traveling pulses are mirror images in $x = 0$. The traveling wave coordinate is

$$(1.2) \quad \xi = x - \Gamma(t) = x - \int_0^t c(s)ds,$$

and the center of the pulse is $\xi = 0$. We thus implicitly assume that the pulse approaches the reflection point $x = 0$ as $t \downarrow 0$, as is the case in the self-replication process [17, 18, 2]. This assumption is not essential; we show in subsection 3.3 how to extend it to describe two-pulse solutions not centered about $x = 0$ on other intervals.

Following the scaling analysis of section 3 in part I, we introduce

$$(1.3) \quad \begin{aligned} \xi &= \sqrt{\frac{D}{B}}\hat{\xi}, & U(x, t) &= U(\xi) = B^{3/2}\sqrt{\frac{D}{A}}\hat{u}(\hat{\xi}), \\ V(x, t) &= V(\xi) = \sqrt{\frac{A}{BD}}\hat{v}(\hat{\xi}), & c(t) &\equiv \frac{A\sqrt{D}}{B^{3/2}}\hat{c}(t). \end{aligned}$$

Also, define the two new small parameters

$$(1.4) \quad \varepsilon = \frac{\sqrt{A}}{B} \quad \text{and} \quad \delta = \sqrt{BD}.$$

System (1.1) now reduces to a four-dimensional *quasi-stationary* system:

$$(1.5) \quad \begin{aligned} \dot{u} &= \varepsilon p, \\ \dot{p} &= \varepsilon \left[uv^2 - \varepsilon Dc(t)p - \varepsilon \delta \left(1 - \frac{\delta}{\varepsilon}u \right) \right], \\ \dot{v} &= q, \\ \dot{q} &= -uv^2 + v - \varepsilon^2 c(t)q, \end{aligned}$$

where we have dropped the hats and where the overdot denotes $d/d\hat{\xi}$. Note that t enters only as a parameter in this ODE.

For $0 < \varepsilon \ll 1$, this system has a well-defined slow-fast structure and can thus be studied by geometric singular perturbation theory [8, 12]. The geometric method employed here extends that used in [2]. There, an invariant slow manifold \mathcal{M} was identified in the phase space of the ODE system for stationary solutions (i.e., $c \equiv 0$ in (1.5)), and the dynamics were decomposed into slow dynamics on \mathcal{M} and fast dynamics in the transverse directions. The same decomposition is made here in (1.5), with several important differences: the pulse is restricted to a semi-infinite ξ -interval, $[\Gamma(t), \infty)$, here so that the two-pulse solution is determined by imposing a homogeneous Neumann boundary condition at the boundary $\xi = -\Gamma(t)$, i.e., $x = 0$, and the solutions here lie exponentially close to the transverse intersections of certain manifolds, instead of in them as in [2].

The geometric singular perturbation approach provides clear insight into the central structures in phase space, as well as into how they vary with parameters. Geometrically, the “fast” V -pulse solutions correspond to the persistent homoclinic orbits to the slow manifold. Also, the dynamics of orbits on the slow manifold \mathcal{M} precisely gives the slow evolution of U outside the pulse intervals. Moreover, the geometric method leads directly to a natural identification of all four subcases Ia–IIb that appeared as algebraic conditions in the analysis of part I. These four conditions on the relative magnitudes of parameters A, B , and D , or equivalently, ε, δ , and D (1.4), can

be interpreted as describing the leading order character of the (linear!) flow on the slow manifold \mathcal{M} (Figure 1(a)–(d)):

$$(1.6) \quad \begin{array}{ll} \text{I: } \sqrt{\frac{B^3 D}{A}} = \frac{\delta}{\varepsilon} \ll 1: & \text{Ia: } \sqrt{\frac{AD}{B^3}} = \frac{\varepsilon D}{\delta} \ll 1 \quad \rightarrow \text{Figure 1a,} \\ & \text{Ib: } \sqrt{\frac{AD}{B^3}} = \frac{\varepsilon D}{\delta} = \mathcal{O}(1) \quad \rightarrow \text{Figure 1b,} \\ \text{II: } \sqrt{\frac{B^3 D}{A}} = \frac{\delta}{\varepsilon} = \mathcal{O}(1): & \text{IIa: } \sqrt{\frac{AD}{B^3}} = \frac{\varepsilon D}{\delta} \ll 1 \quad \rightarrow \text{Figure 1c,} \\ & \text{IIb: } \sqrt{\frac{AD}{B^3}} = \frac{\varepsilon D}{\delta} = \mathcal{O}(1) \quad \rightarrow \text{Figure 1d.} \end{array}$$

In part I, we constructed only the slowly modulated two-pulse solutions in case Ia. Here, we will first use the geometric approach as a natural tool to analyze traveling pulse solutions in this same “basic” case. As a result, we will obtain a full understanding of the observed maximum wave speeds. Next, we will study the other, limiting or bifurcation, case Ib, in which classical traveling waves with $c \equiv c_0$ exist, and case IIa in which the two-pulse solutions disappear in a saddle-node bifurcation. Furthermore, we will show how the geometric approach can be used to demonstrate that the solutions constructed in part I actually exist as solutions of the PDE; see section 3.4.

Next, we show how our analysis in parts I and II leads to results for the splitting bifurcation, by continuing them into the regime $\varepsilon = \sqrt{A/B} = \mathcal{O}(1)$ where the start of the self-replication process is observed. First, in the special scaling used in [2, 3], it was already found that there are critical values of the ratio A/B^2 , called $\varepsilon_{\text{split}}$ in this paper, at which the stationary one-pulse solutions (Figure 3 in part I) “disappear.” This “disappearance bifurcation” was identified as a saddle-node bifurcation of homoclinic orbits in the numerical simulations of [16]. The existence of this disappearance or saddle-node bifurcation value for $A/B^2 = \varepsilon_{\text{split}}$ was proven by a topological shooting method in [3] for a certain special scaling of A , B , and D . The analysis carries over almost verbatim for the general problem studied here.

Taking this verbatim extension as the basis for further analysis, we argue here that there is an “effective” scaled value, $\varepsilon = \varepsilon(t)$, of the ratio A/B^2 that varies slowly in time. When the two pulses are close together, i.e., just after the splitting of the stationary one-pulse pattern (Figure 1 in part I), this effective value is less than the unscaled ratio A/B^2 of the one-pulse. Therefore, the two-pulse pattern can exist when the one-pulse has already “disappeared”: the splitting process has effectively reduced A/B^2 below $\varepsilon_{\text{split}}$. However, $\varepsilon(t)$ increases slowly toward the unscaled ratio A/B^2 associated with the one-pulse pattern; and hence, at a certain time, $\varepsilon(t)$ will pass through $\varepsilon_{\text{split}}$ and the two slowly traveling pulses will both split; see Figures 1 and 2 in part I. These arguments also predict that the structure of the traveling pulse solutions between successive splittings must be structurally different when A/B^2 is not close to $\varepsilon_{\text{split}}$. This is confirmed by numerical simulations.

An overview of the existence and stability results obtained in both parts of this work is given in Figure 2 when $0 < D \ll 1$. This case is the most natural one in light of the stability results of part I (the slowly modulated pulses are unstable for $D \geq \mathcal{O}(1)$) and the validity analysis of the quasi-stationary approach in subsection 3.4. However, we emphasize that, for instance, the existence results for stationary pulses in part I (and in [2]) are also valid for $D \geq \mathcal{O}(1)$. The various curves marking the bifurcations (section 4) and stability boundaries (part I) are shown in the two parameter (α, β) -space where $A = D^\alpha$ and $B = D^\beta$. The curves \mathcal{C}_{TW} and \mathcal{C}_{SN} , respectively, correspond to cases Ib and IIa and are thus to be interpreted in terms of the dynamics on the slow manifold; see (1.6), Figure 1, and Remark 1.3.

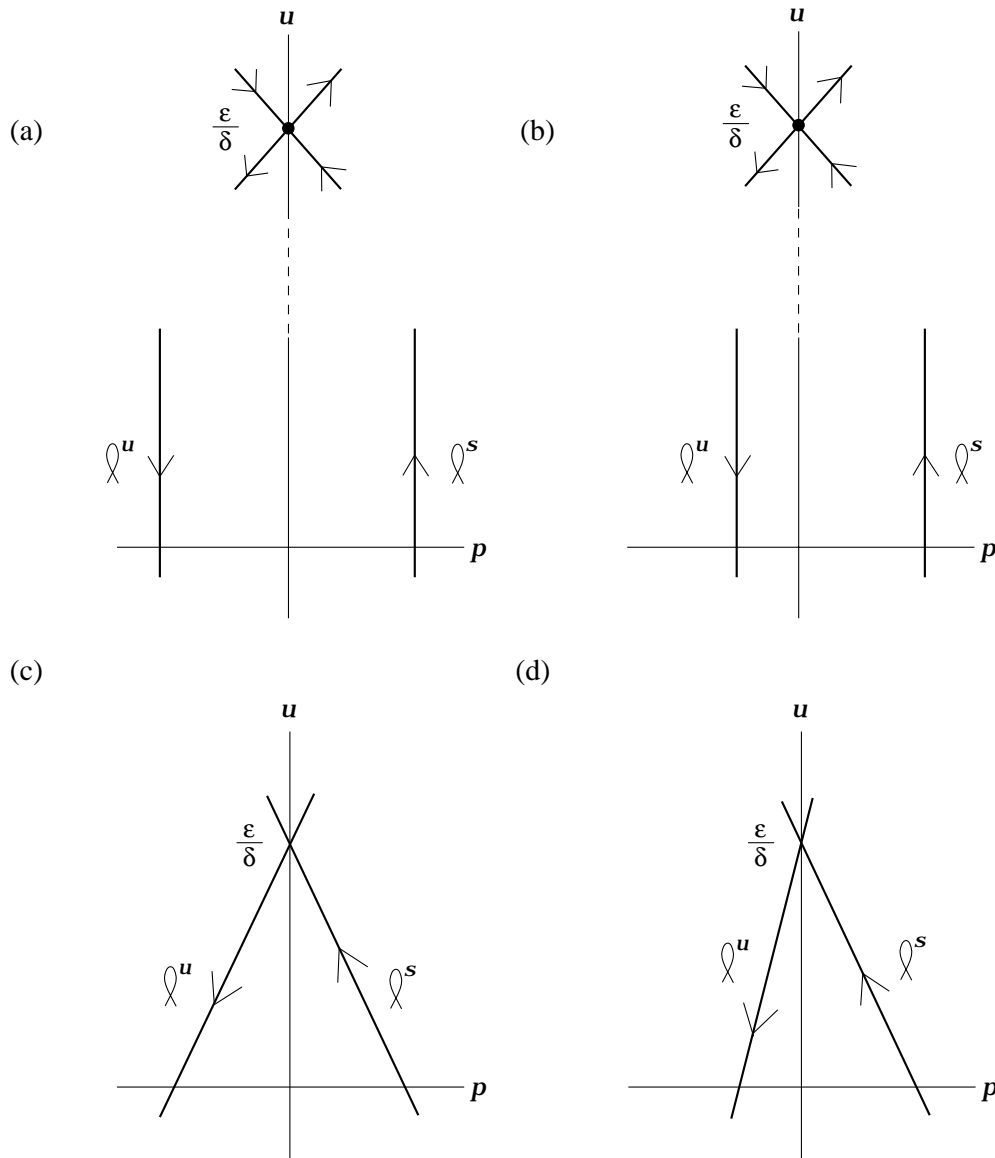


FIG. 1. A schematic illustration of the geometries on the slow manifolds in each of the four distinct subcases identified in this paper. Frames (a)–(d) correspond to subcases Ia–IIb, respectively. In (a) and (b), the dashed segment on the u -axis indicates that $\epsilon/\delta \gg 1$. In (a) and (c), the restricted manifolds ℓ^U and ℓ^S are symmetric about the u -axis, whereas they are not symmetric in frames (b) and (d).

This paper is organized as follows. In section 2, we present the fundamental geometric properties of (1.5). The basic slowly modulated two-pulse solution, case Ia, is constructed in section 3. In section 3, we also consider the bounded interval and asymmetric cases, and we establish the validity of the quasi-stationary approach. Cases Ib and IIa are considered in section 4. The implications of the analytical results for the understanding of the self-replicating process and the essential role of the slowly varying $U(x, t)$ in this process are discussed in section 5. Finally, in section 6, we relate

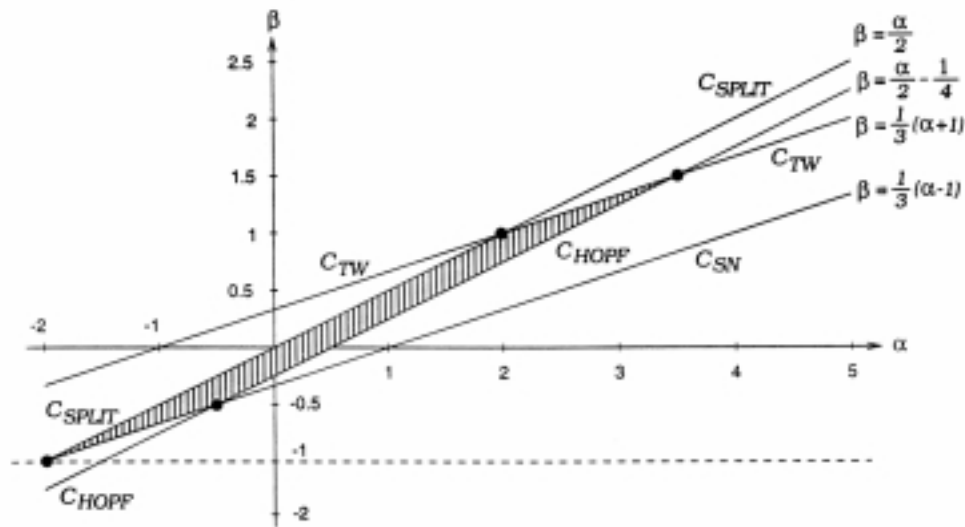


FIG. 2. A summary of the existence and stability results obtained in this paper, shown in the limit $0 < D \ll 1$. The scalings $A = D^\alpha$ and $B = D^\beta$ are used for this figure only. The lines shown are C_{SN} : $\beta = (\alpha/3) - (1/3)$ (case IIa); C_{SPLIT} : $\beta = \alpha/2$ (see 1.4 and section 5); C_{TW} : $\beta = (\alpha/3) + (1/3)$ (case Ib); and, C_{HOPF} : $\beta = (\alpha/2) - (1/4)$ at which the pulse solutions lose their stability through a Hopf bifurcation. See part I.

this work to literature on self-replication.

Remark 1.1. ε^2 and δ^2 here are the parameters λ and γ in [10]. The δ in [10] differs from the δ here. Also, in [10], $\lambda\gamma = 1$ or close to 1, while here $\varepsilon^2\delta^2 \ll 1$.

Remark 1.2. The methods developed here also apply to “mildly strong” interactions of multipulse solutions in general singular reaction-diffusion equations, including the (generalized) Gierer–Meinhardt model [4, 15]; see [5].

Remark 1.3. The decisive influence of the character of the dynamics on the slow manifold on the existence and the dynamics of “localized structures” in singular perturbed reaction-diffusion equations has been studied in more detail in [11].

2. Geometry of governing equations.

2.1. Dynamics on the slow manifold. In (1.5), for any ε , the plane $\mathcal{M} \equiv \{(u, p, v, q) | v, q = 0\}$ is invariant under the flow of (1.5). Thus, the dynamics of the system decompose naturally into a slow part (on \mathcal{M}) and a fast part (off of \mathcal{M}). The dynamics on \mathcal{M} are given by the reduced slow system, and this system is linear:

$$(2.1) \quad \dot{u} = \varepsilon p, \quad \dot{p} = -\varepsilon^2 Dc(t)p - \varepsilon^2 \delta \left(1 - \frac{\delta}{\varepsilon} u \right).$$

The homogeneous steady state ($U = 1, V = 0$) corresponds to the saddle fixed point $S = (u = \varepsilon/\delta, p = 0, v = 0, q = 0)$ on the manifold \mathcal{M} . Therefore, there is one major difference between cases I and II (1.6) that manifests itself already, namely, the u component of S satisfies $u \gg 1$ in case I, whereas $u = \mathcal{O}(1)$ in case II. See Figure 1.

Exploring further, the eigenvalues of the reduced slow system at S are

$$(2.2) \quad \lambda_{\pm} = -\frac{\varepsilon^2 Dc}{2} \pm \delta\varepsilon \sqrt{1 + \frac{\varepsilon^2 D^2 c^2}{4\delta^2}}.$$

Hence, the restricted stable and unstable manifolds of S are the lines

$$(2.3) \quad W^S(S)|_{\mathcal{M}} \equiv \ell^S : p = \frac{\lambda_+}{\varepsilon} \left(u - \frac{\varepsilon}{\delta} \right), \quad W^U(S)|_{\mathcal{M}} \equiv \ell^U : p = \frac{\lambda_-}{\varepsilon} \left(u - \frac{\varepsilon}{\delta} \right).$$

As we show now on a case-by-case basis, these formulae reveal that in case I, the lines ℓ^S and ℓ^U are asymptotically vertical, whereas they have a much smaller (albeit still $\mathcal{O}(1/\varepsilon)$) slope in case II. Then, in subcase a, the lines ℓ^S and ℓ^U are symmetric about the u -axis, while they are asymmetric about the u -axis in subcase b. Hence, there are four geometrically distinct combinations; see Figure 1.

In case Ia, i.e., when $\delta/\varepsilon \ll 1$ and $\varepsilon D/\delta \ll 1$, we find

$$(2.4) \quad \lambda_{\pm} = \pm \varepsilon \delta + \text{h.o.t.},$$

so that the restricted stable and unstable manifolds of S are the lines

$$(2.5) \quad W^S(S)|_{\mathcal{M}} \equiv \ell^S : p = \varepsilon - \delta u + \text{h.o.t.}, \quad W^U(S)|_{\mathcal{M}} \equiv \ell^U : p = -\varepsilon + \delta u + \text{h.o.t.}$$

These lines are asymptotically vertical in the $p-u$ plane in the region where $u = \mathcal{O}(1)$ when $\delta/\varepsilon \ll 1$ (see Figure 1(a)) and ℓ^U and ℓ^S are symmetric with respect to the u axis.

In case Ib, i.e., when $\delta/\varepsilon \ll 1$ but now $\varepsilon D/\delta = \mathcal{O}(1)$, all of the terms in the expression (2.2) for the eigenvalues are of leading order. Let $\gamma \equiv \varepsilon D/\delta$ so that $\gamma = \mathcal{O}(1)$. Then, (2.2) yields

$$(2.6) \quad \lambda_{\pm} = \varepsilon \delta \tilde{\lambda}_{\pm} = \varepsilon \delta \left[-\frac{1}{2} \gamma c \pm \sqrt{1 + \frac{1}{4} \gamma^2 c^2} \right].$$

Thus, ℓ^S and ℓ^U are given exactly by

$$(2.7) \quad p = -\tilde{\lambda}_{\pm} (\varepsilon - \delta u),$$

and the first term is the leading order term when $u = \mathcal{O}(1)$ because $\delta/\varepsilon \ll 1$. Therefore, ℓ^S and ℓ^U are vertical lines to leading order for $u = \mathcal{O}(1)$. However, they are no longer symmetric about the u -axis due to the difference in the magnitudes of $\tilde{\lambda}_{\pm}$; see Figure 1(b). This complicates the analysis considerably, as we show in subsection 4.1.

In case IIa, the saddle fixed point is located only an $\mathcal{O}(1)$ distance from the origin along the u -axis, since $\delta/\varepsilon = \mathcal{O}(1)$. Hence, the lines ℓ^S and ℓ^U have much smaller slope (“only $\mathcal{O}(1/\varepsilon)$ ”) than in case I. In addition, since $\varepsilon D/\delta \ll 1$ here, these lines are again symmetric about the u -axis:

$$(2.8) \quad p = \pm \varepsilon (1 - \sigma u),$$

where $\sigma = \delta/\varepsilon$ is an $\mathcal{O}(1)$ parameter. See Figure 1(c). Finally, in going to case IIb, we see that the lines become asymmetric about the u -axis. In both subcases IIa and IIb, there are saddle-node bifurcations of the modulated pulse solutions.

Remark 2.1. We do not pay any attention to case IIb in this paper. This is in essence a codimension two case that can be studied by combining cases Ib and IIa, which are represented by the curves \mathcal{C}_{SN} and \mathcal{C}_{TW} , respectively, in Figure 2. Moreover, the combination of $\delta/\varepsilon = \mathcal{O}(1)$ and of $\varepsilon D/\delta = \mathcal{O}(1)$ implies that $D = \mathcal{O}(1)$. Hence, $\mathcal{C}_{\text{SN}} \cap \mathcal{C}_{\text{TW}} = \emptyset$ in Figure 1 since there $D \ll 1$. The case $D = \mathcal{O}(1)$ is of little interest in light of the stability analysis of section 4 in part I.

2.2. The fast subsystem when $\varepsilon = 0$. The fast subsystem is obtained from (1.5) by noting that u and p remain constant when $\varepsilon = 0$:

$$(2.9) \quad \dot{v} = q, \quad \dot{q} = -uv^2 + v.$$

This reduced fast subsystem is Hamiltonian for each constant u with $K = q^2/2 + uv^3/3 - v^2/2$. For each positive u , the phase portrait of (2.9) has a center equilibrium at $(\frac{1}{u}, 0)$ and a saddle equilibrium at $(0, 0)$ that possesses an orbit homoclinic to it:

$$(2.10) \quad v_0(\xi; u) = \frac{3}{2u} \operatorname{sech}^2\left(\frac{\xi}{2}\right) \quad \text{and} \quad q_0(\xi; u) = \dot{v}_0,$$

where v_0 here differs slightly from \hat{v}_0 used in part I. See also Figure 3a in [2].

Let \mathcal{M}_0 denote the two-dimensional plane $\mathcal{M}_0 \equiv \{(u, p, v, q) \mid v, q = 0\}$ obtained in the $\varepsilon = 0$ limit. It coincides with \mathcal{M} , and the subscript just reminds us that $\varepsilon = 0$ in this subsection. That the origin $(v = 0, q = 0)$ is a saddle point of the reduced fast system for each positive value of the constant u immediately implies that \mathcal{M}_0 is an invariant manifold and that it is normally hyperbolic. Over each point $(u, p, 0, 0)$ on \mathcal{M}_0 there are one-dimensional fast stable and unstable fibers; these correspond precisely to the local stable and unstable manifolds of the saddle point $(v = 0, q = 0)$ of the fast subsystem. Hence, when $u > 0$, the manifold \mathcal{M}_0 has three-dimensional stable and unstable manifolds, $W^S(\mathcal{M}_0)$ and $W^U(\mathcal{M}_0)$, that are simply the unions of the above one-dimensional fibers over the two-dimensional set of base points $(u, p, 0, 0)$ on \mathcal{M}_0 . Moreover, since these local manifolds coincide in the fast subsystem to form the homoclinic orbit given by (2.10), it follows directly that each point on \mathcal{M}_0 is connected to itself by a homoclinic orbit and that the manifold \mathcal{M}_0 possesses a three-dimensional homoclinic manifold $W(\mathcal{M}_0)$.

2.3. Persistent fast connections. Fenichel theory [8] implies that the stable and unstable manifolds of \mathcal{M} present in the $\varepsilon = 0$ system persist as three-dimensional, C^r smooth stable and unstable manifolds, $W^U(\mathcal{M})$ and $W^S(\mathcal{M})$, for $0 < \varepsilon \ll 1$. See also Theorem 3 of [12]. However, the branches of these manifolds that coincided when $\varepsilon = 0$ generally no longer do so and intersect each other in two-dimensional surfaces. In these intersections lie the only one-pulse orbits biasymptotic to \mathcal{M} .

We employ a Melnikov method to detect these intersections. Robinson’s extension of the Melnikov method applies to system (1.5); see [21]. Let $(u(\xi), p(\xi), v(\xi), q(\xi))$ be a solution of (1.5) that passes through the point $(u_0, p_0, v(0), 0)$ when $\xi = 0$. The splitting distance between the manifolds $W^U(\mathcal{M})$ and $W^S(\mathcal{M})$ can be measured in the hyperplane $\{q = 0\}$: the hyperplane transverse to $W(\mathcal{M})$ and spanned by the three vectors $(1, 0, 0, 0)$, $(0, 1, 0, 0)$, and $\hat{n} = (0, 0, 1, 0)$ to $W(\mathcal{M}_0)$. The distance is

$$(2.11) \quad \Delta K(u_0, p_0; a, b, c) \equiv \int_{-\infty}^{\infty} \dot{K}(v(\xi), q(\xi); u(\xi), p(\xi)) d\xi$$

as $\varepsilon \rightarrow 0^+$, and the integrand is $\dot{K} = \frac{1}{3}\varepsilon p v^3 - \varepsilon^2 c(t) q^2$.

Solutions $(u(\xi), p(\xi), v(\xi), q(\xi))$ of (1.5) on the perturbed manifolds $W^S(\mathcal{M})$ and $W^U(\mathcal{M})$ can be expanded in powers of the small parameter ε as $\varepsilon \rightarrow 0$:

$$(2.12) \quad \begin{aligned} u(\xi) &= u_0 + \varepsilon u_1(\xi) + \varepsilon^2 u_2(\xi) + \text{h.o.t.}, \\ p(\xi) &= p_0 + \varepsilon p_1(\xi) + \varepsilon^2 p_2(\xi) + \text{h.o.t.}, \\ v(\xi) &= v_0(\xi; u_0) + \varepsilon v_1(\xi) + \varepsilon^2 v_2(\xi) + \text{h.o.t.}, \\ q(\xi) &= q_0(\xi; u_0) + \varepsilon q_1(\xi) + \varepsilon^2 q_2(\xi) + \text{h.o.t.}, \end{aligned}$$

where $v_0(\xi; u_0)$ is the unperturbed homoclinic solution (2.10). The expansions for solutions on $W^U(\mathcal{M})$ are valid on $(-\infty, 0]$, and the expansions for solutions on $W^S(\mathcal{M})$ are valid on $[0, \infty)$.

We fix initial conditions on the curves $W^S(\mathcal{M}) \cap \{q = 0\}$ and $W^U(\mathcal{M}) \cap \{q = 0\}$ whose v -coordinates lie in a neighborhood of $3/(2u)$. We assume that $u(0) = u_0$ and $u_j(0) = 0$ for $j \geq 1$: the initial conditions $p_0, p_j(0)$, and $v_j(0)$ ($j \geq 1$) are then determined as functions of u_0 by the condition that the orbit of $(u(\xi), p(\xi), v(\xi), q(\xi))$ lies in the transverse intersection of $W^S(\mathcal{M})$ and $W^U(\mathcal{M})$. We label such an orbit $\Gamma(\xi; x_0)$, where $x_0 = (u_0, p(0), v(0), 0)$.

One observes straightaway that $p_0 = 0$, since the p -coordinates of all points on ℓ^S and ℓ^U with u -coordinate of size $\mathcal{O}(1)$ are at most $\mathcal{O}(\varepsilon)$ in magnitude (see (2.5)), and hence the only way for the initial conditions x_0 to lead to an orbit that is either forward or backward asymptotic to S is if $p(0) = \mathcal{O}(\varepsilon)$. Also, the first-order corrections of u and p are found by substituting (2.12) into (1.5):

$$(2.13) \quad u_1(\xi) \equiv 0, \quad p_1(\xi) = \int_0^\xi u_0 v_0^2(s) ds + p_1(0).$$

Hence, the integral in $p_1(\xi)$ is odd in ξ , because $v_0(\xi)$ is even in ξ . Plugging these expansions into \dot{K} and (2.11) and using odd-even properties yields to leading order

$$(2.14) \quad \Delta K(u_0, p(0); a, b, c(t)) = \varepsilon^2 \left[\frac{1}{3} p_1(0) \int_{-\infty}^\infty v_0^3(\xi) d\xi - c(t) \int_{-\infty}^\infty q_0^2(\xi) d\xi \right].$$

Therefore, using (2.10), the zero set of ΔK is given to leading order by the line

$$(2.15) \quad p = \frac{1}{2} \varepsilon c u,$$

where we recall u is assumed $\mathcal{O}(1)$. Hence, there exist initial conditions $x_0 = (u_0, p(0), v(0), 0)$ such that the orbits $\Gamma(\xi; x_0)$ through these points are biasymptotic to \mathcal{M} if the u - and p -coordinates of the initial conditions chosen above are related to leading order as in (2.15) with $p = \mathcal{O}(\varepsilon)$. Also, as $c \rightarrow 0^+$, the zero line of ΔK approaches the vertical; see Remark 3.2.

In order to quantify the influence of the fast field on the u - and p -coordinates of a solution in $W^U(\mathcal{M}) \cap W^S(\mathcal{M})$ during its excursion through the fast field, we define

$$\Delta p(u_0, p(0); a, b, c(t)) \equiv \int_{-\infty}^\infty \dot{p} d\xi \quad \text{and} \quad \Delta u(u_0, p(0); a, b, c(t)) \equiv \int_{-\infty}^\infty \dot{u} d\xi.$$

Before evaluating these expressions, we note that $\Delta K = \mathcal{O}(\varepsilon^2)$ implies $|v(0) - v_0| = \mathcal{O}(\varepsilon^2)$. Hence, $v_1(\xi) \equiv 0$, since v_1 is the solution of a second-order equation with initial conditions $v_1(0), \dot{v}_1(0) = 0$. Straightforward computations now give

$$(2.16) \quad \Delta p = \varepsilon \int_{-\infty}^\infty (uv^2 + \text{h.o.t.}) d\xi = \varepsilon \int_{-\infty}^\infty u_0 v_0^2 d\xi + \text{h.o.t.} = \varepsilon \frac{6}{u_0} + \text{h.o.t.},$$

where we have also used (1.5), (2.13), and the fact that $\int_{-\infty}^\infty v_0^2(\xi) d\xi = 6/u_0^2$.

Finally, to determine the change in u during the fast field, we again use the fact that we will study only $\Delta u(u_0, p(0))$ for values of $(u_0, p(0))$ in the neighborhood of the $\Delta K = 0$ line (2.15). As above, therefore, $p(\xi) = \mathcal{O}(\varepsilon)$ on the time interval under consideration. Hence, the change in u during the excursion in the fast field is

$$(2.17) \quad \Delta u = \mathcal{O}(\varepsilon^2).$$

2.4. Takeoff and touchdown curves. There are two other curves on \mathcal{M} that play a crucial role in the analysis. These are obtained as follows. The first intersection of $W^S(\mathcal{M})$ and $W^U(\mathcal{M})$ in the hyperplane $\{q = 0\}$ is given by (2.15) to leading order. This intersection is a one-dimensional curve in the two-dimensional manifold $W^S(\mathcal{M}) \cap W^U(\mathcal{M})$. Through any point x_0 on this curve $W^S(\mathcal{M}) \cap W^U(\mathcal{M}) \cap \{q = 0\}$ there is an orbit $\Gamma(\xi; x_0)$ which approaches \mathcal{M} for “large” $|\xi|$. More precisely, the Fenichel theory [8] implies that for any $\Gamma(\xi; x_0)$ there are two orbits $\Gamma_{\mathcal{M}}^+ = \Gamma_{\mathcal{M}}^+(\xi; x_0^+) \subset \mathcal{M}$ and $\Gamma_{\mathcal{M}}^- = \Gamma_{\mathcal{M}}^-(\xi; x_0^-) \subset \mathcal{M}$, respectively (where $\Gamma^+(0; x_0^+) = x_0^+ \in \mathcal{M}$), such that $\|\Gamma(\xi; x_0) - \Gamma_{\mathcal{M}}^+(\xi; x_0^+)\|$ is exponentially small for $\xi > 0$ where $t \geq \mathcal{O}(\frac{1}{\varepsilon})$ and $\|\Gamma(\xi; x_0) - \Gamma_{\mathcal{M}}^-(\xi; x_0^-)\|$ is exponentially small for $-\xi \geq \frac{K}{\varepsilon} > 0$. Thus, for some $k > 0$,

$$d(\Gamma(\xi; x_0), \mathcal{M}) = \mathcal{O}\left(e^{-\frac{k}{\varepsilon}}\right) \text{ for } |\xi| \geq \mathcal{O}\left(\frac{1}{\varepsilon}\right) \text{ or larger}$$

and $\Gamma_{\mathcal{M}}^{\pm}(\xi; x_0^{\pm})$ determine the behavior of $\Gamma(\xi; x_0)$ near \mathcal{M} . These are the orbits of the base points of the fast stable and unstable fibers in whose intersection Γ lies.

Therefore, we define the curves $T_o \subset \mathcal{M}$ (takeoff) and $T_d \subset \mathcal{M}$ (touchdown) as

$$(2.18) \quad T_o = \cup_{x_0} \{x_0^- = \Gamma_{\mathcal{M}}^-(0; x_0^-)\}, \quad \text{and} \quad T_d = \cup_{x_0} \{x_0^+ = \Gamma_{\mathcal{M}}^+(0; x_0^+)\},$$

where the unions are over all x_0 in $W^S(\mathcal{M}) \cap W^U(\mathcal{M}) \cap \{q = 0\}$. T_o (respectively, T_d) is the collection of base points of all of the fibers in $W^U(\mathcal{M})$ (respectively, $W^S(\mathcal{M})$) that lie in the transverse intersection of $W^U(\mathcal{M})$ and $W^S(\mathcal{M})$.

The locations of T_o and T_d can be obtained explicitly by determining the relations between $x_0 = (u_0, p(0), v(0), 0)$ and $x_0^{\pm} = (u_0^{\pm}, p_0^{\pm}, 0, 0)$. The accumulated changes in p of $\Gamma(t)$ during the backward and forward (half-circuit) excursions through the fast field are measured by $\int_{-\infty}^0 \dot{p} d\xi$ and $\int_0^{\infty} \dot{p} d\xi$, respectively. The changes in p of $\Gamma^{\pm}(t)$ during the same period of time can be neglected, to leading order, since $\dot{p} = \mathcal{O}(\varepsilon^3)$ on \mathcal{M} by (1.5). Formulae (1.5) and (2.17) imply $u_0 = u_0^{\pm}$ to leading order. Therefore, by the same calculations that led to (2.15) and (2.16), one finds to leading order

$$(2.19) \quad T_o : p = \frac{1}{2}\varepsilon \left[cu - \frac{6}{u} \right], \quad T_d : p = \frac{1}{2}\varepsilon \left[cu + \frac{6}{u} \right].$$

3. Geometric construction of slowly modulated two-pulse solutions. In this section, we construct slowly modulated two-pulse solutions in case Ia by “hooking up” the fast and slow components of the geometric approach. The ODE for $c(t)$ is derived in subsection 3.2. The influence of a restriction to a bounded interval is briefly discussed in section 3.3. In subsection 3.4, we establish the validity of the quasi-stationary approximation used throughout both parts of this work.

3.1. The right-moving pulse with slowly changing $c(t)$: Hooking up the slow and fast segments. In this subsection, we construct instantaneous (fixed t) snapshots of the right-moving pulse solution on $x \geq 0$. As stated above, at any instant of time t , this solution consists of three segments, and we start with the slow segment to the right of the peak. These instantaneous t snapshots are then put together in subsection 3.2. We reintroduce hats on the independent variable ξ where appropriate in this section.

For instantaneous wave speeds satisfying $0 < c(t) < 1/6$, the curve T_d on \mathcal{M} intersects the line ℓ^S in two distinct points. The leading order analysis in (2.5) and

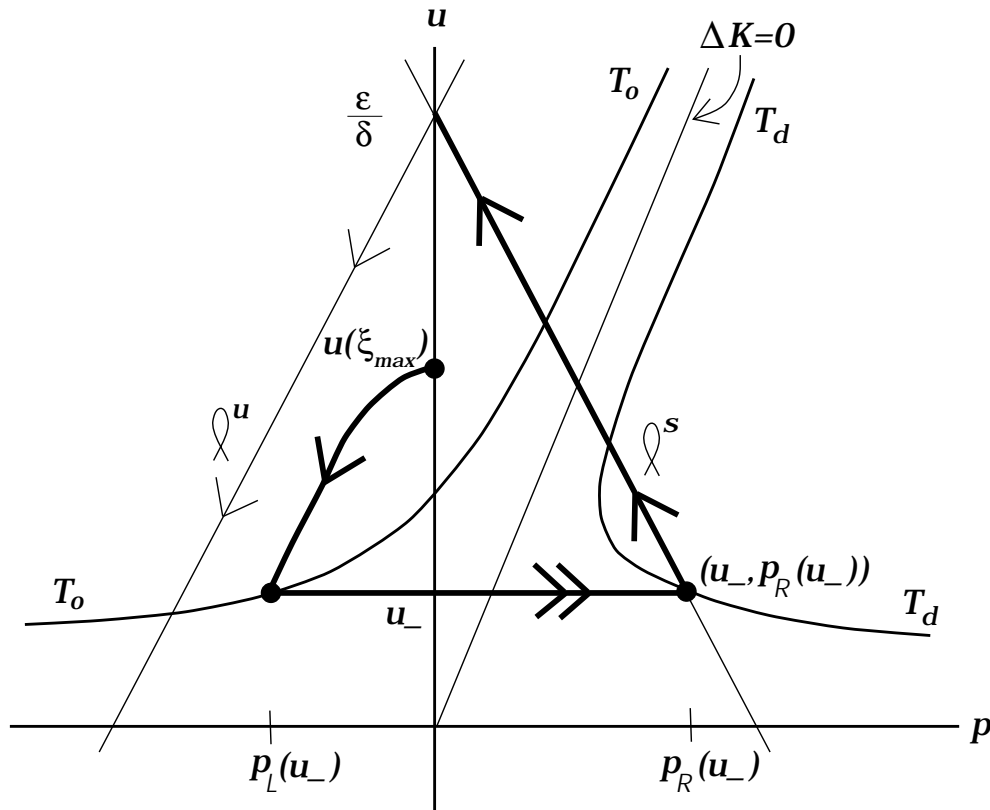


FIG. 3. A schematic illustration of the rightward moving slowly modulated pulse in the phase space of the ODE (1.5) at a fixed instant of time t . The thickest curve corresponds to the singular orbit for the slowly modulated pulse with the horizontal segment being a projection of the homoclinic excursion in the fast field onto the slow manifold \mathcal{M} . The curves T_o and T_d , as well as the restricted stable and unstable manifolds ℓ^S and ℓ^U , are also shown.

(2.19) directly yields that the upper and lower intersection points are $(u_{\pm}, p_R(u_{\pm}))$:

$$(3.1) \quad u_{\pm} = \frac{1}{c(t)} \left(1 \pm \sqrt{1 - 6c(t)} \right),$$

and $p_R(u_{\pm})$ is given to leading order by the first term in the first equation in (2.5). See Figure 3. We note that $du_-/dc > 0$ for all $c > 0$. This leading order analysis also identifies the critical (maximum) wave speed as $c(t) = 1/6$. At this $c(t)$ value, the two curves are tangent, and it represents to leading order the initial value of the wave speed of the pulses with slowly decreasing wave speed.

To leading order, the right slow segment we are interested in is given by the orbit along that segment of ℓ^S from $u = u_-$ to $u = \varepsilon/\delta$. This right slow segment satisfies the asymptotic condition $U \rightarrow 1$ because the solution on ℓ^S approaches S , i.e., $u \rightarrow \varepsilon/\delta$ and $p \rightarrow 0$. See Figure 3. The v - and q -coordinates are exponentially small, and hence zero to leading order and to all orders.

At the intersection point $(u_-, p_R(u_-))$, the right slow segment is hooked up to the fast segment. This fast segment is given to leading order by the homoclinic orbit (2.10) of the fast reduced system (2.9) with $\varepsilon = 0$, where the constant u , and hence also the u component of the initial condition, are fixed at u_- . See Figure 3. That

these solution segments can be hooked up smoothly in this fashion for the full system with $0 < \varepsilon \ll 1$ is justified by the fact that, for $c < 1/6$, the curves T_d and ℓ^S intersect transversely on \mathcal{M} at $(u_-, p_R(u_-))$, and hence the geometric singular perturbation theory of Fenichel may be applied; see [8] and [12].

The backward asymptotic ($\hat{\xi} \rightarrow -\infty$) limit set of the fast homoclinic pulse is the point $(u_-, p_L(u_-))$ on \mathcal{M} . We use (2.5) and (2.19) to compute to leading order

$$(3.2) \quad p_L(u_-) = p_R(u_-) - \Delta p(u_-) = \varepsilon \left(1 - \frac{6}{u_-} \right) = -\varepsilon \sqrt{1 - 6c(t)}.$$

See Figure 3. The point $(u_-, p_L(u_-))$ lies on the takeoff curve T_o , and the result (3.2) expresses the fact that the jump from T_o (namely, $(u_-, p_L(u_-))$) to T_d (namely, $(u_-, p_R(u_-))$) during the fast segment is given to leading order by the accumulated change $\Delta p(u_-)$ in p , where u stays constant to a sufficiently high order by (2.17). For $0 < c(t) < 1/6$, the point $(u_-, p_L(u_-))$ lies to the right ℓ^U , inside the triangle formed by these lines and the p -axis, whereas it lies on ℓ^U for $c = 0$; see [2].

The identification of $(u_-, p_L(u_-))$ completes the specification of the fast segment and it is precisely at this point that we hook up the fast segment to the left slow segment. To leading order, the left slow solution is the segment of a hyperbolic cosine orbit on \mathcal{M} (inside the triangle) between the points $(u_{\max}, 0)$ and $(u_-, p_L(u_-))$. See Figure 3. The u component is given to leading order by

$$(3.3) \quad u(\hat{\xi}) = \frac{\varepsilon}{\delta} + \mathcal{A}e^{\varepsilon\delta\hat{\xi}} + \mathcal{B}e^{-\varepsilon\delta\hat{\xi}},$$

where the unknown coefficients are determined by imposing the two given boundary conditions. Without loss of generality, since the ODE system is autonomous in ξ (and $\hat{\xi}$), we are free to choose the parametrization such that $(u(\xi), p(\xi))|_{\xi=0} = (u_-, p_L(u_-))$. Hence, we impose $u(\xi = 0) = u_-$ and $\frac{du}{d\xi}(\xi = 0) = \varepsilon p_L(u_-)$, which yields

$$\mathcal{A} + \mathcal{B} = -\frac{\varepsilon}{\delta} + \mathcal{O}(1) \quad \text{and} \quad \mathcal{A} - \mathcal{B} = -\frac{\varepsilon}{\delta} \sqrt{1 - 6c(t)} + \mathcal{O}(1).$$

Note we used that $u_- = \mathcal{O}(1)$ by (3.1) and that $p_L(u_-) = \mathcal{O}(\varepsilon)$ by (3.2), while $\varepsilon/\delta \gg 1$. Therefore, letting $H \equiv \sqrt{1 - 6c(t)}$, we obtain

$$(3.4) \quad \begin{aligned} u(\hat{\xi}) &= \frac{\varepsilon}{2\delta} \left[2 - (1 + H)e^{\varepsilon\delta\hat{\xi}} + (H - 1)e^{-\varepsilon\delta\hat{\xi}} \right] + \text{h.o.t.}, \\ p(\hat{\xi}) &= -\frac{\varepsilon}{2} \left[(1 + H)e^{\varepsilon\delta\hat{\xi}} + (H - 1)e^{-\varepsilon\delta\hat{\xi}} \right] + \text{h.o.t.} \end{aligned}$$

Thus, the left slow segment satisfies the left boundary condition $du/dx = 0$ at $x = 0$ for our right-moving pulse solution at every instant of time t . In the full system, the hooking up of the left slow segment and the fast segment is justified in the same way as that done for the right slow segment.

Finally, with this solution in hand, we can calculate the value of $\hat{\xi}$ at which the slow segment begins, i.e., at which $u(\hat{\xi}) = u_{\max}$ and $p(\hat{\xi}) = 0$. We label this value $\hat{\xi}_{\max}$. It is negative and equal to $\Gamma(t)$ from section 3. See Figure 3. In particular, by imposing $p(\hat{\xi}_{\max}) = 0$ in (3.4)(b), one finds to leading order

$$(3.5) \quad \hat{\xi}_{\max} = \frac{1}{2\varepsilon\delta} \ln \left(\frac{1 - H}{1 + H} \right).$$

Recalling $u_{\max} = \mathcal{O}(\varepsilon/\delta)$ (1.3) and combining (3.4) and (3.5) yield

$$(3.6) \quad u_{\max}(t) \stackrel{\text{def}}{=} \frac{\varepsilon}{\delta} U_{\max}(t) = \frac{\varepsilon}{\delta} \left(1 - \sqrt{6\hat{c}(t)} \right).$$

Thus, $U_{\max}(t) = U(0, t)$, the unscaled value of the solution $U(x, t)$ of (1.1) at $x = 0$ (see Figure 1 in part I). Below we will find that $\hat{c}(t) \in (0, 1/6)$, i.e., $U_{\max}(t) \in (0, 1)$. These last formulae (3.5) and (3.6) complete our leading order description of the right moving pulse solution on the domain $x \geq 0$ at each instant of time t with $c(t)$ as yet unknown. The solution on $x \leq 0$ at the same instant of time t is determined by reflecting the solution on $x \geq 0$ across $x = 0$.

Remark 3.1. The above analysis specifies the leading order solution for the right moving pulse. When $0 < \varepsilon \ll 1$, this solution is in $W^S(\mathcal{M})$ and lies exponentially close to the transverse intersection of the local manifolds $W_{\text{loc}}^U(\mathcal{M})$ and $W_{\text{loc}}^S(\mathcal{M})$. Also, as $\hat{\xi}$ decreases to $\hat{\xi}_{\max}$, the orbit comes exponentially close to \mathcal{M} with exponentially small (but nonzero) V component.

3.2. The ODE for $c(t)$ in case Ia. In this subsection, we determine the explicit formula for the slow rate of change of $c(t)$. This will complete our existence proof of the full right moving pulse solution with slowly decreasing wave speed in case Ia. In this subsection, we will again put a hat on the variable c where appropriate.

Recall from (1.2) that the traveling wave variable was defined as $\xi = x - \int_0^t c(s) ds$, where ξ and c are unscaled. Plugging in the scalings for ξ and c given by (1.3), respectively, and evaluating at $x = 0$ (i.e., at $\xi = \xi_{\max} = -\int_0^t c(s) ds < 0$), one finds

$$(3.7) \quad \hat{\xi}_{\max} = \frac{-\varepsilon^2 \delta^2}{D} \int_0^t \hat{c}(s) ds.$$

At each fixed instant of time t , this value of $\hat{\xi}_{\max}$ represents precisely the distance between the origin ($x = 0$) and the center of the peak. Moreover, this value (3.7) must agree with (3.5). Hence, equating (3.5) and (3.7) yields

$$(3.8) \quad \ln \left(\frac{1 - \sqrt{1 - 6\hat{c}(t)}}{1 + \sqrt{1 - 6\hat{c}(t)}} \right) = \frac{-2\varepsilon^3 \delta^3}{D} \int_0^t \hat{c}(s) ds,$$

where we recall that the parameter H introduced there is defined in terms of \hat{c} . Finally, differentiating both sides of (3.8) with respect to t yields the desired ODE

$$(3.9) \quad \frac{d\hat{c}}{dt} = \frac{-2\varepsilon^3 \delta^3 \hat{c}^2}{D} \sqrt{1 - 6\hat{c}},$$

which is exactly the same as the ODE (3.32) found in part I (use (1.3) and (1.4)). Hence, $\hat{c} = 1/6$ is an unstable fixed point and that the existence of this critical maximum value of \hat{c} has a clear geometric origin, namely, it is the \hat{c} value at which T_d is tangent to ℓ^S . Also, since $d\hat{c}/dt$ scales as $-\hat{c}^2$ for small \hat{c} , we know \hat{c} decays as $1/t$.

Remark 3.2. The $c = 0$ case is treated explicitly in [2], and one must take into account higher-order terms here when analyzing the transition from $c > 0$ to $c = 0$.

Remark 3.3. Using the same procedure employed above, we can also show that the above-type two-pulse solutions with u near u_+ , the second solution in (3.1), in the fast field do not exist. In particular, since $p_R(u_+) = \varepsilon$ to leading order, $p_L(u_+) = p_R(u_+) - \Delta p(u_+) = \varepsilon[1 - (6/u_+)] = \varepsilon H$, where we recall $H = \sqrt{1 - 6c}$. Hence,

$p_L(u_+) > 0$ for all $0 \leq c \leq 1/6$, and one cannot hook up the fast jump to a slow (cosh-type) solution that reaches $p = 0$ for some $\hat{\xi}_{\max} < 0$.

Remark 3.4. In the formula (4.12) for $\Delta_s u_\xi$ in [1] the limits were inadvertently switched, although the reported value is correct.

3.3. Bounded domains and N -pulse solutions ($N \neq 2$). So far we have focused on the construction of two-pulse solutions on an unbounded domain. As a consequence, we could assume that the two-pulse pattern is symmetric with respect to the point $x = 0$ that is exactly between the two pulses. This is technically the simplest case and for that reason we present only the details of this case in this work.

However, the geometric approach developed in this paper can also be applied to “mildly strong” pulse dynamics of N -pulses on bounded (or unbounded) domains without a symmetry. As an example, we briefly discuss the case of a one-pulse pattern on a bounded domain $[0, L]$ with homogeneous Neumann boundary conditions. We assume that the “fast” pulse is initially centered around the point $x_{\text{init}} \in [0, L]$. As before we formulate the system in traveling coordinates by introducing $\xi = x - \Gamma(t)$ with $\Gamma(t) = x_{\text{init}} + \int_0^t c(s) ds$ so that the center of the pulse is at $\xi = 0$ ($x = \Gamma(t)$) for all $t \geq 0$. The main difference with the situation studied in the previous (sub)sections is that the boundary condition $U \rightarrow 1$ as $\xi \rightarrow \infty$ now must be replaced by $\partial U / \partial \xi = 0$ at $\xi = L - \Gamma(t)$. However, this situation is in essence the same as that at the left-hand side of the pulse in the previous subsections. The application of the boundary conditions on both ξ -intervals $[-\Gamma(t), 0]$ and $[0, L - \Gamma(t)]$ determine two segments of hyperbolic cosine orbits (as (3.3)) on \mathcal{M} . Thus, the main difference between this “bounded” case and that of the previous subsections is that the projection on \mathcal{M} of the slowly modulated pulse solution now consists of two hyperbolic cosine orbits instead of one to the left of the pulse and ℓ^S to the right (Figure 3). This has no influence on the method. As before, the speed $c(t)$ is determined by the condition that the solution must “jump” through the fast field from the “end” of the left orbit (where $U = \mathcal{O}(\delta/\varepsilon)$ (1.3), (1.4)) to the “beginning” of the right orbit. Next, one can derive an ODE for $c(t)$ by the same consistency condition as above. This ODE shows that $\Gamma(t) \rightarrow \frac{1}{2}L$ as $t \rightarrow \infty$, i.e., the pulse moves toward the middle of the interval with decreasing speed, in full agreement with numerical simulations.

The “mildly strong” interactions of more than 1 (in general N) pulses on a bounded or unbounded interval can be studied along the same lines: the U -components of the solution in between two pulses are determined by the slow flow (and the “boundary conditions”), and the ODE that describes the speed $c_i(t)$ of each individual pulse follows from the combination of a “jump condition” and a “consistency condition.”

In the case of a symmetric two-pulse solution on the bounded interval $[0, L]$, the analysis shows that it converges toward the (asymptotically stable) stationary periodic two-pulse solution [3, 13] with pulses at $L/4$ and at $3L/4$, as confirmed by numerics.

Remark 3.5. The above sketched method can also be used to study the dynamics of the four-pulse solution that appears from the second splitting (i.e., the first splitting of the traveling two-pulse), or to the multipulse solutions that appear after the subsequent pulse splittings (see Figure 2 in part I and Figure 4).

3.4. The validity of the quasi-stationary approach. In this subsection, the validity of the quasi-stationary approach is analyzed. We begin by observing that a smooth solution of the full PDE (1.1) must satisfy

$$(3.10) \quad \left. \begin{aligned} \lim_{x \uparrow 0} \frac{\partial^k}{\partial x^k} U(x, t) &= \lim_{x \downarrow 0} \frac{\partial^k}{\partial x^k} U(x, t) \\ \lim_{x \uparrow 0} \frac{\partial^k}{\partial x^k} V(x, t) &= \lim_{x \downarrow 0} \frac{\partial^k}{\partial x^k} V(x, t) \end{aligned} \right\} \text{ for all } t \geq 0, k \geq 0.$$

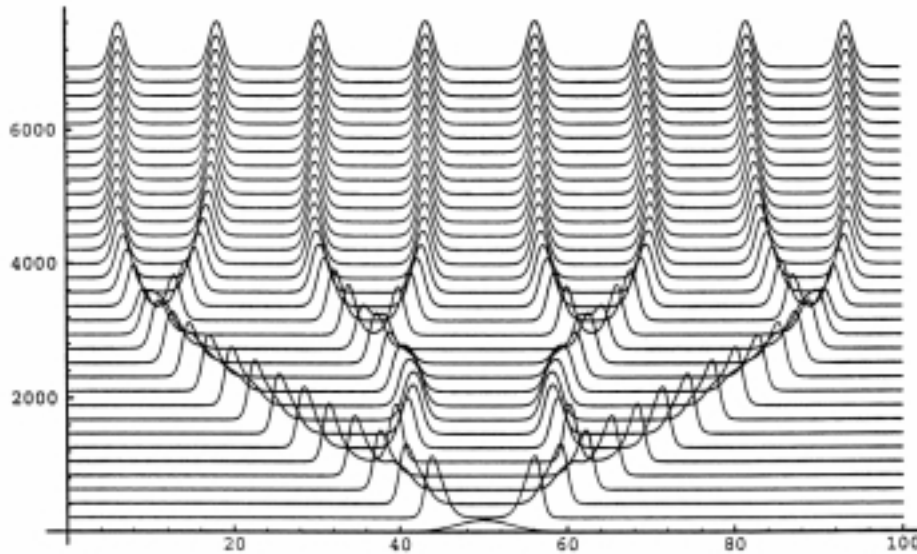


FIG. 4. Time evolution of the V component of a modulated two-pulse solution of (1.1) with $A = 0.01$, $B = 0.0474$, and $D = 0.01$, so that ε lies not “close” to $\varepsilon_{\text{split}}$. The outermost pulses appear to propagate at constant speed while significant oscillations take place on the trailing edges before the splitting. The vertical axis is $700V + t$.

Moreover, the reversibility symmetry of (1.1) implies that all odd derivatives at $x = 0$ vanish (the two-pulse solution is even as function of x). The slowly modulated two-pulse solutions have been constructed and uniquely determined in the ODE (1.5) by imposing only a condition on the $\partial U/\partial x$ at $x = 0$ (and one as $x, \xi \rightarrow \infty$). We now show that the third-order derivative of U at $x = 0$, as well as all odd higher-order spatial derivatives there, are small, but nonzero, for the leading order approximation obtained from the quasi-stationary analysis. In addition, we show that the reintroduction of the explicit (and higher-order) time derivative terms remedies this defect and results in a smooth and consistent solution of the full PDE (1.1).

The quasi-stationary approach implies that one assumes that $(U(x, t), V(x, t)) = (u(\xi_r(t)), v(\xi_r(t)))$ for $x \geq 0$, and $(U(x, t), V(x, t)) = (u(\xi_l(t)), v(\xi_l(t)))$ for $x \leq 0$ (to leading order), where $\xi_r(t) = x - \Gamma(t) = x - \int_0^t c(s)ds$ (for $x \geq 0$) and $\xi_l(t) = x + \Gamma(t)$ (for $x \leq 0$). The boundary conditions (3.10) for u become

$$(3.11) \quad \begin{aligned} \frac{\partial^{2m}}{\partial \xi_r^{2m}} u(\xi_r)|_{\xi_r = -\Gamma(t)} &= \frac{\partial^{2m}}{\partial \xi_l^{2m}} u(\xi_l)|_{\xi_l = \Gamma(t)}, \\ \frac{\partial^{2n+1}}{\partial \xi_r^{2n+1}} u(\xi_r)|_{\xi_r = -\Gamma(t)} &= \frac{\partial^{2n+1}}{\partial \xi_l^{2n+1}} u(\xi_l)|_{\xi_l = \Gamma(t)} = 0 \end{aligned}$$

for all $m, n \geq 0$ and $t \geq 0$, where only the conditions involving $m, n = 0$ were used in the construction of the two-pulse solutions. Also, the conditions on $v(\xi_{r,l})$ may be ignored here, since v and its derivatives are exponentially small near $x = 0$.

Now, it is a straightforward computation to check that

$$(3.12) \quad \begin{aligned} \frac{\partial^2}{\partial \xi_r^2} u(-\Gamma(t)) &= \frac{\partial^2}{\partial \xi_l^2} u(\Gamma(t)) = -A(1 - U_{\max}(t)), \\ \frac{\partial^3}{\partial \xi_r^3} u(-\Gamma(t)) &= -\frac{\partial^3}{\partial \xi_l^3} u(\Gamma(t)) = c(t)A(1 - U_{\max}(t)) \neq 0, \end{aligned}$$

where $U_{\max}(t) = u(\xi_r)|_{\xi_r=-\Gamma(t)} = u(\xi_l)|_{\xi_l=\Gamma(t)}$; see (3.6). Thus, it follows immediately that, while the first condition in (3.11) is satisfied for $m = 1$, there is a “jump” in the third derivative at $x = 0$ and the second condition in (3.11) is not satisfied for $n = 1$:

$$(3.13) \quad \Delta \frac{\partial^3 U}{\partial \hat{\xi}^3} = \mathcal{O}\left(\frac{A^2 D^2}{B^3}\right) = \mathcal{O}(\varepsilon^4 \delta D) \ll 1,$$

where we have used the proper scales for the spatial variable $\hat{\xi}_{r,l}$ (1.3) and the wave speed c (1.3), as well as (1.4). Moreover, there are jumps in all of the higher-order odd derivatives at $x = 0$. Therefore, the leading order quasi-stationary approximation has a defect in that it does not give a smooth solution of the PDE (1.1). This defect is inherent in the leading order approximation, since the pulses are determined up to all orders in the perturbation expansion by the $m, n = 0$ boundary conditions (3.11) applied to the ODE (1.5), and hence there is no “freedom” left in the ODE reduction to satisfy the other boundary conditions with $m > 0, n > 0$.

To remedy this defect in the leading order quasi-stationary approximation, we introduce a *slow* time variable and consider the explicit time dependence

$$(3.14) \quad \tau = \left(\frac{A}{B}\right)^{\frac{3}{2}} \sqrt{Dt} = \frac{\varepsilon^3 \delta^3}{D} t,$$

$$(3.15) \quad \begin{aligned} (U(x, t), V(x, t)) &= (U(\xi_r(\tau), \tau), V(\xi_r(\tau), \tau)) \quad \text{for } x \geq 0, \\ (U(x, t), V(x, t)) &= (U(\xi_l(\tau), \tau), V(\xi_l(\tau), \tau)) \quad \text{for } x \leq 0. \end{aligned}$$

The slow time variable τ makes it explicit that (U, V) evolves on the same (slow) time scale as c and U_{\max} (see (3.6)). The choice (3.14) can also be obtained by taking a general scaling for τ and then determining its “significant degeneration”; see [6].

Working explicitly on the domain $x > 0$ and with the right moving pulse (i.e., using $\xi = \xi_r$), the boundary condition at $x = 0$ is

$$(3.16) \quad U(-\Gamma(\tau), \tau) \stackrel{\text{def}}{=} U_{\max}(\tau), \quad \text{and} \quad U_\xi(-\Gamma(\tau), \tau) = 0 \quad \text{for all } \tau \geq 0.$$

Now, assuming that $V(\xi(\tau), \tau)$ is negligible near $x = 0$ (like $v(\xi(\tau))$ in the ODE) and that the $U_{\max}(\tau)$ is the same (to leading order) as the one determined by the ODE approach, one finds

$$(3.17) \quad \frac{\partial}{\partial \tau} U(\xi_r = -\Gamma, \tau) = \frac{d}{d\tau} U_{\max}(\tau)$$

(see (3.9) and (3.6) for the explicit leading order expression), and a similar expression can be obtained for the left moving pulse.

Remark 3.6. At this stage, one still has to check for consistency whether the explicit dependence of U, V on τ only has a higher-order influence on the behavior of $U(\xi(\tau), \tau)$ and $V(\xi(\tau), \tau)$ compared to $u(\xi(\tau))$ and $v(\xi(\tau))$ (for all x , not only near $x = 0$).

With the formula (3.17), one verifies that the first boundary condition in (3.11) is still satisfied with $m = 1$. In particular, by evaluating all of the terms in the PDE for the U components of the solutions (3.15) at $\xi_r = -\Gamma(t)$ and at $\xi_l = \Gamma(t)$ and by neglecting terms involving $V(\xi, \tau)$, $V_\tau(\xi, \tau)$, and their derivatives with respect to ξ , which are all exponentially small in a neighborhood of $x = 0$, we find

$$(3.18) \quad \frac{\partial^2}{\partial \xi_r^2} U(-\Gamma(\tau), \tau) = \frac{\partial^2}{\partial \xi_l^2} U(\Gamma(\tau), \tau) = \frac{d}{d\tau} U_{\max}(\tau) - A(1 - U_{\max}(\tau)).$$

Finally, by differentiating the PDE for U once with respect to ξ and again neglecting exponentially small terms, we deduce the desired result,

$$(3.19) \quad \frac{\partial^3}{\partial \xi_r^3} U(-\Gamma(\tau), \tau) = \frac{\partial^3}{\partial \xi_l^3} U(\Gamma(\tau), \tau) = 0,$$

since differentiation of the second condition in (3.16) with respect to τ and use of the chain rule reveals that $U_{\xi_r, \tau}(-\Gamma(\tau), \tau) = c(\tau)U_{\xi_r, \xi_r}(-\Gamma(\tau), \tau)$, and a similar equality holds for the solution on $x < 0$. Similarly, one shows that all of the higher-order derivatives of $(U(\xi_r(\tau), \tau), V(\xi_r(\tau), \tau))$ and $(U(\xi_l(\tau), \tau), V(\xi_l(\tau), \tau))$ are equal at $x = 0$, i.e., that $(U(\xi_{r,l}(\tau), \tau), V(\xi_{r,l}(\tau), \tau))$ satisfies the boundary conditions (3.10), (3.11) for all $m, n \geq 0$. Therefore, with the higher-order terms included, the quasi-stationary approximation (3.15) is smooth at $x = 0$ to all orders.

We conclude this section by showing that the improved quasi-stationary approximation is *consistent*, i.e., introduction of the explicit temporal behavior does not influence the ODE methods of the previous sections to leading order. We scale $(U(\xi(\tau), \tau), V(\xi(\tau), \tau))$ into $(\hat{U}(\hat{\xi}(\tau), \tau), \hat{V}(\hat{\xi}(\tau), \tau))$, precisely as in (1.3), and we use (1.4) and (3.14) to write the PDE for (\hat{U}, \hat{V}) in the form of the ODE for (\hat{u}, \hat{v}) (1.5) associated with the leading order quasi-stationary approximation (for $\xi = \xi_r$, i.e., $x \geq 0$):

$$(3.20) \quad \begin{aligned} \hat{U}_\xi &= \varepsilon \hat{P}, \\ \hat{P}_\xi &= \varepsilon \left[\hat{U} \hat{V}^2 - \varepsilon D \hat{c}(\tau) \hat{P} - \varepsilon \delta \left(1 - \frac{\delta}{\varepsilon} \hat{U} + D \hat{U}_\tau \right) \right], \\ \hat{V}_\xi &= \hat{Q}, \\ \hat{Q}_\xi &= -\hat{U} \hat{V}^2 + \hat{V} - \varepsilon^2 \hat{c}(\tau) \hat{Q} + \varepsilon^3 \delta \hat{V}_\tau. \end{aligned}$$

The invariant slow manifold \mathcal{M} of the ODE (1.5) persists, along with its fast stable and unstable manifolds. Moreover, since the manifolds $W^S(\mathcal{M})$ and $W^U(\mathcal{M})$ intersect transversely in the phase space of the original ODE, the smallness of the coefficients in front of the \hat{U}_τ and the \hat{V}_τ terms imply that they continue to intersect in (3.20). Hence, the geometric singular perturbation analysis by which the traveling pulses are constructed is not influenced by these terms, and the ‘‘PDE contributions’’ \hat{U}_τ and \hat{V}_τ cannot have a leading order effect on the analysis. However, the term $D \hat{U}_\tau$ will have a leading order effect on the flow on \mathcal{M} when $D \geq \mathcal{O}(1)$. Hence, the improved quasi-stationary approach will a priori be consistent only when we impose that $D \ll 1$. We have found in part I that the stationary one-pulses can only be stable when $D \ll 1$. Since the modulated two-pulses solutions converge to two copies of these stationary one-pulses ($c \rightarrow 0$ if $t \rightarrow \infty$), there is no reason to expect that the case $D \geq \mathcal{O}(1)$ will be relevant in the analysis the two-pulse solutions.

Thus, the improved quasi-stationary approach is consistent: the leading order behavior of (U, V) is given by the solution (u, v) determined by the ODE dynamics

(and thus it follows for instance that $V(x, t)$ is exponentially small near $x = 0$) and the transition from $x \leq 0$ to $x \geq 0$ is smooth. The validity of the improved quasi-stationary approximation can now be proved by a combination of the transversality results of the geometric analysis (see [8, 12]) and by explicitly showing that \hat{U}_τ and \hat{V}_τ are both $\mathcal{O}(1)$. We do not consider the details any further here.

4. Geometric constructions of two-pulse solutions: Cases Ib and IIa.

4.1. Case Ib: $\varepsilon D/\delta = \mathcal{O}(1)$, the bifurcation of traveling waves. In this subsection, we study the existence of slowly modulated two-pulse solutions in case Ib, i.e., in that part of parameter space where $\delta/\varepsilon \ll 1$ but $\varepsilon D/\delta = \mathcal{O}(1)$. We will find that the slowly modulated solutions exist only for $\varepsilon D/\delta < 3$ and that there exist critical constant values of $c \neq c(t)$ for which “classical” traveling waves exist. These values of c will later be interpreted as critical points of the ODE for $c(t)$.

A modulated traveling wave corresponds to an orbit that is asymptotically close to ℓ^U for $\xi \ll -1$ and to ℓ^S for $\xi \gg 1$. These orbits lie exponentially close to intersections $\ell^U \cap T_o$ and $\ell^S \cap T_d$ with the same u -coordinates (since u does not change (to leading order) after one circuit through the fast field (2.17)). Note that T_o and T_d are still given by (2.19). Thus, combining (2.19) with (2.7), we obtain

$$(4.1) \quad -\tilde{\lambda}_- = \frac{1}{2} \left[cu - \frac{6}{u} \right], \quad -\tilde{\lambda}_+ = \frac{1}{2} \left[cu + \frac{6}{u} \right].$$

By (2.6), this immediately yields that either $c = 0$ or $u = \gamma$ (recall that $\gamma = \varepsilon D/\delta = \mathcal{O}(1)$). The first solution, $c = 0$, corresponds to the stationary waves of section 2, while the second solution, $u = \gamma$, yields

$$(4.2) \quad c = \pm c_c(\gamma) = \pm \frac{2}{\gamma} \sqrt{\frac{9}{\gamma^2} - 1}.$$

At $\gamma = 3$ the traveling waves collide in a pitchfork bifurcation. Below we will show that the slowly modulated traveling waves also disappear in this pitchfork bifurcation.

The construction of the slowly modulated waves closely follows that of the previous subsections. The points $(u_\pm, p_R(u_\pm))$ at which ℓ^S and T_d intersect are

$$(4.3) \quad u_\pm = \frac{1}{c} \left[-\tilde{\lambda}_- \pm \sqrt{\tilde{\lambda}_-^2 - 6c} \right],$$

where the condition $\tilde{\lambda}_-^2 - 6c \geq 0$ again gives an upper bound c_{\max} on c (ℓ^S and T_d are tangent at $c = c_{\max}$). Again, only the lower intersection point $(u_-, p_L(u_-))$ can be the basis of the construction of the modulated wave. This point determines the touchdown point of an orbit that takes off at the point $(u_-, p_L(u_-))$, where, by (2.19),

$$p_L(u_-) = \frac{1}{2} \varepsilon \left(cu_- - \frac{6}{u_-} \right) = -\varepsilon \sqrt{\tilde{\lambda}_-^2 - 6c}.$$

The final segment of the singular solution is the left slow orbit segment on \mathcal{M} given by the solution of (2.1) when $\varepsilon D/\delta = \gamma$. Its general solution is

$$(4.4) \quad \begin{pmatrix} u(\xi) \\ p(\xi) \end{pmatrix} = \mathcal{A} e^{\varepsilon \delta \tilde{\lambda}_+ \xi} \begin{pmatrix} 1 \\ \delta \tilde{\lambda}_+ \end{pmatrix} + \mathcal{B} e^{\varepsilon \delta \tilde{\lambda}_- \xi} \begin{pmatrix} 1 \\ \delta \tilde{\lambda}_- \end{pmatrix} + \begin{pmatrix} \varepsilon/\delta \\ 0 \end{pmatrix}.$$

Imposing the initial condition $(u(0), p(0)) = (u_-, p_L(u_-))$ yields, to leading order,

$$(4.5) \quad \mathcal{A} = \frac{\varepsilon}{\delta} \left(\frac{\tilde{\lambda}_- - \sqrt{\tilde{\lambda}_-^2 - 6c}}{\tilde{\lambda}_+ - \tilde{\lambda}_-} \right), \quad \mathcal{B} = -\frac{\varepsilon}{\delta} \left(\frac{\tilde{\lambda}_+ - \sqrt{\tilde{\lambda}_+^2 - 6c}}{\tilde{\lambda}_+ - \tilde{\lambda}_-} \right).$$

We proceed by determining the “time” $\xi = \xi_{\max}$ at which we have $p(\xi) = 0$ (the Neumann boundary condition on the full solution at $x = 0$; see Figure 3),

$$(4.6) \quad \xi_{\max} = \frac{-1}{2\varepsilon\delta\sqrt{1 + \frac{1}{4}\gamma^2c^2}} \ln \left[\frac{\tilde{\lambda}_-(\tilde{\lambda}_+ - \sqrt{\tilde{\lambda}_-^2 - 6c})}{\tilde{\lambda}_+(\tilde{\lambda}_- - \sqrt{\tilde{\lambda}_-^2 - 6c})} \right],$$

and one readily verifies that when $\gamma \rightarrow 0$ this reduces to the value of $\hat{\xi}_{\max}$ calculated in (3.5) of subsection 3.1 (where $\gamma \ll 1$). However, in this more general case, we need to impose an extra condition on c , since it is not clear that ξ_{\max} exists. In other words, the condition on c follows from the geometrical observation that the slow segment on \mathcal{M} through $(u_-, p_L(u_-))$ only intersects the $\{p = 0\}$ -axis when $(u_-, p_L(u_-))$ lies between ℓ^U and ℓ^S (see Figure 3). From (2.6) and (4.6) we see that only one term in the log function can change sign. Thus, the existence of ξ_{\max} is equivalent to

$$(4.7) \quad \tilde{\lambda}_+ - \sqrt{\tilde{\lambda}_-^2 - 6c} \geq 0, \quad \text{i.e.,} \quad -c_c(\gamma) \leq c(t) \leq c_c(\gamma).$$

As a consequence, there are no slowly modulated traveling waves for $\gamma \geq 3$, ($\varepsilon D/\delta \geq 3$). In Figure 2, the line labeled C_{TW} marks the bifurcation in which these traveling waves are created. It is given by $\beta = (\alpha/3) + (1/3)$, where we recall that for the purposes of Figure 2, $A = D^\alpha$ and $B = D^\beta$.

Assuming that (4.7) holds, we obtain the equation for $c(t)$ by equating the above ξ_{\max} with the distance traveled by the pulse (given in (3.7)):

$$(4.8) \quad \ln \left[\frac{\tilde{\lambda}_-(\tilde{\lambda}_+ - \sqrt{\tilde{\lambda}_-^2 - 6\hat{c}})}{\tilde{\lambda}_+(\tilde{\lambda}_- - \sqrt{\tilde{\lambda}_-^2 - 6\hat{c}})} \right] = \frac{-2}{\gamma} \varepsilon^4 \delta^2 \sqrt{1 + \frac{1}{4}\gamma^2\hat{c}^2} \int_0^t \hat{c}(s) ds,$$

where we have reintroduced the “hats” on the $c(t) = \hat{c}(t)$ for clarity. Note that $\tilde{\lambda}_\pm = \tilde{\lambda}_\pm(\hat{c}(t))$ (2.6): it is possible to rewrite this equation into a differential equation for $\hat{c}(t)$ (by differentiation, as in subsection 3.2), but in this case the expression will be so complicated that it becomes prohibitive to gain additional insight into $\hat{c}(t)$.

Instead, we confine ourselves to answering two standard questions for autonomous first order ODEs: what are the critical points, and since the stable critical points are the only possible attractors, which are stable? Since the right-hand side of (4.8) becomes unbounded as $\hat{c}(t) \rightarrow \hat{c}_0$, a constant, it follows that the critical points are given by $\tilde{\lambda}_+ - \sqrt{\tilde{\lambda}_-^2 - 6c} = 0$. Thus, once again, $\hat{c}_0 = 0, \pm c_c(\gamma)$. Inserting $\hat{c} = \tilde{c} \ll 1$ in (4.8) yields the “linearization”

$$\ln \left[\frac{1}{2}(3 - \gamma)\tilde{c} \right] = -2\varepsilon^4 \delta^2 \int_0^t \tilde{c}(s) ds.$$

Thus, by differentiation, $\hat{c}_0 = 0$ is stable, and it follows that as long as the slowly modulated waves exist (i.e., $\gamma < 3$), they will evolve toward the stationary wave as $t \rightarrow \infty$. Moreover, the other two critical points, $\hat{c}_0 = \pm c_c$, are unstable.

Remark 4.1. The existence result for traveling waves for $\varepsilon D/\delta = \mathcal{O}(1)$, or by (1.4) $AD = \mathcal{O}(B^3)$, does not contradict the nonexistence result for traveling waves in [2]: there A, B , and D are scaled as $D = \delta^2 \ll 1, A = a\delta^2, B = b\delta^\beta, \beta \in [0, 1)$ so that $AD \ll B^3$. We refer to [14] for the construction of different types of traveling waves.

4.2. Case IIa: $\delta/\varepsilon = \mathcal{O}(1)$, a saddle-node bifurcation of two-pulse solutions. In this subsection, we establish the existence of a pair of slowly modulated two-pulse solutions in case IIa, i.e., when $\delta/\varepsilon = \mathcal{O}(1)$ and $\varepsilon D/\delta \ll 1$. We employ the same method as used in section 3 and in subsection 4.1, stating only the essential steps. As in the previous section we will find that the modulated two-pulse solutions exist only up to a critical value. We define a new, $\mathcal{O}(1)$ parameter σ by $\delta = \sigma\varepsilon$ and find that the modulated pulse solutions can exist only up to $\sigma = 1/12$. At this critical value the pulse solutions merge in a homoclinic saddle-node bifurcation. Geometrically this means that, in \mathcal{M} , ℓ^S and T_d are tangent at this value of σ (with $c = 0$); $\ell^S \cap T_d = \emptyset$ when $\sigma > 1/12$ so that there can neither be slowly modulated nor stationary pulse solutions for $\sigma > 1/12$. See the curve labeled \mathcal{C}_{SN} in Figure 2, which is determined by $\beta = (\alpha/3) - (1/3)$, since $\delta/\varepsilon = \mathcal{O}(1)$ here (and $A = D^\alpha$ and $B = D^\beta$ for the purposes of Figure 2). This saddle-node bifurcation has already been studied for the stationary pulses in subsection 4.3 of [2].

On the slow manifold \mathcal{M} , the saddle fixed point is now at $(u = 1/\sigma, p = 0)$, and its restricted unstable and stable manifolds are given by

$$(4.9) \quad \ell^{U,S} : \quad p = \mp\varepsilon [1 - \sigma u] + \text{h.o.t.}$$

Therefore, the term linear in u is also of leading order, whereas it was of higher order in cases Ia and Ib. Next, the zero set of ΔK is given by the line (2.15) here, just as it was in subsection 3.2, the jump in p during the fast field is also determined by (2.16), and finally the takeoff and touchdown curves are given by (2.19) in this case, as well, all to leading order.

Due to the difference in the position of the line ℓ^S between this case and those encountered in cases Ia and Ib, the points $(u_\pm, p_R(u_\pm))$ on \mathcal{M} at which ℓ^S intersects T_d are located at different points from that given in subsection 3.1 (3.1):

$$(4.10) \quad u_\pm = \frac{1 \pm \sqrt{1 - 6c - 12\sigma}}{c + 2\sigma}.$$

Hence, (4.10) reveals that, in order for the intersection points to exist, one needs

$$(4.11) \quad 1 - 6c - 12\sigma > 0.$$

Otherwise, ℓ^S and T_d are tangent (or do not intersect) when $1 - 6c - 12\sigma = 0 (< 0)$. Moreover, (4.10) identifies the maximum wave speed $c(t)$ as

$$(4.12) \quad c_{\max} = \frac{1}{6} - 2\sigma,$$

and, consequently, the interval $0 < \sigma < 1/12$ corresponds to the interval in which the slowly modulated two-pulse solutions exist with positive wave speed. Finally, the lower intersection point $(u_-, p_L(u_-))$ exhibits the following asymptotics:

$$(4.13) \quad u_- \rightarrow \begin{cases} \frac{1 - \sqrt{1 - 12\sigma}}{2\sigma} & \text{as } c \rightarrow 0^+, \\ \frac{1}{6} & \text{as } c \rightarrow c_{\max}. \end{cases}$$

Having obtained the information about the lower intersection point, we now proceed to piece together the right slow, fast, and left slow segments of the instantaneous (frozen $c(t)$) pulse solution on the domain $x \geq 0$, as in subsection 3.1. Inserting the above formula (4.10) for u_- into (2.8) for the line ℓ^S yields

$$p_R(u_-) = \varepsilon(1 - \sigma u_-) = \varepsilon \left[1 - \sigma \left(\frac{1 - \tilde{H}}{c + 2\sigma} \right) \right],$$

where we define $\tilde{H} \equiv \sqrt{1 - 6c - 12\sigma}$ in analogy with the expression H in subsection 3.1. For simplifying the further computations, we note that $c + 2\sigma = (1 - \tilde{H}^2)/6$. Next, we identify the alpha-limit set of the reduced fast homoclinic pulse, which is the point $(u_-, p_L(u_-))$ on T_o , where

$$(4.14) \quad p_L(u_-) = p_R(u_-) - \Delta p(u_-) = -\varepsilon \left(\tilde{H} + \frac{6\sigma}{1 + \tilde{H}} \right)$$

since $\Delta p(u_-) = 6\varepsilon/u_-$. This point on the takeoff curve lies on a hyperbolic cosine solution on \mathcal{M} inside the triangle formed by S , ℓ^U , ℓ^S and the p -axis:

$$u(\hat{\xi}) = \frac{1}{\sigma} + \mathcal{A}e^{\varepsilon^2\sigma\hat{\xi}} + \mathcal{B}e^{-\varepsilon^2\sigma\hat{\xi}}.$$

Imposing $(u(\hat{\xi} = 0), p(\hat{\xi} = 0)) = (u_-, p_L(u_-))$, as before, we find to leading order

$$\mathcal{A} + \mathcal{B} = \frac{-1}{\sigma} + \frac{6}{1 + \tilde{H}} \quad \text{and} \quad \mathcal{A} - \mathcal{B} = - \left(\frac{\tilde{H}}{\sigma} + \frac{6}{1 + \tilde{H}} \right).$$

Therefore, to leading order the slow solution is

$$(4.15) \quad \begin{aligned} u(\hat{\xi}) &= \frac{1}{2\sigma} \left[2 - (1 + \tilde{H})e^{\varepsilon^2\sigma\hat{\xi}} + \left(\tilde{H} - 1 + \frac{12\sigma}{1 + \tilde{H}} \right) e^{-\varepsilon^2\sigma\hat{\xi}} \right], \\ p(\hat{\xi}) &= \frac{-\varepsilon}{2} \left[(1 + \tilde{H})e^{\varepsilon^2\sigma\hat{\xi}} + \left(\tilde{H} - 1 + \frac{12\sigma}{1 + \tilde{H}} \right) e^{-\varepsilon^2\sigma\hat{\xi}} \right]. \end{aligned}$$

Hence, the desired time of flight along the slow manifold \mathcal{M} for the slow segment to reach the u -axis, where $p = 0$ and u is a maximum, is given explicitly by

$$(4.16) \quad \hat{\xi}_{\max} = \frac{1}{2\varepsilon^2\sigma} \ln \left(\frac{1 - \tilde{H}}{1 + \tilde{H}} - \frac{12\sigma}{(1 + \tilde{H})^2} \right).$$

The second expression for this same time of flight comes, just as in subsection 3.2, from recalling the initial setup of the traveling wave variable: $\xi = x - \int_0^t c(s)ds$ and the subsequently introduced scalings, so that at $x = 0$, we have

$$(4.17) \quad \hat{\xi}_{\max} = \frac{-\varepsilon^4\sigma^2}{D} \int_0^t \hat{c}(s)ds.$$

Therefore, upon equating these two expressions (4.16) and (4.17) for $\hat{\xi}_{\max}$, we have the desired (implicit) equation that determines $\hat{c}(t)$:

$$(4.18) \quad \ln \left(\frac{1 - \tilde{H}^2 - 12\sigma}{(1 + \tilde{H})^2} \right) = \frac{-2\varepsilon^6\sigma^3}{D} \int_0^t \hat{c}(s)ds.$$

Differentiating (4.18) with respect to t (and doing a little algebra) yields

$$(4.19) \quad \frac{d\hat{c}}{dt} = \frac{-2\varepsilon^6\sigma^3}{D}\hat{c}^2\sqrt{1-6\hat{c}-12\sigma}\left(\frac{\hat{c}+2\sigma}{\hat{c}+2\sigma\sqrt{1-6\hat{c}-12\sigma}}\right).$$

The additional terms in (4.19) compared to (3.9) do not influence the qualitative behavior of $\hat{c}(t)$: there is an upper bound on \hat{c} that is approached as t becomes small and $\hat{c} \rightarrow 0$ monotonically (as $1/t$) when $t \rightarrow \infty$. Moreover, one can recover (3.9) from (4.19) by replacing σ with δ/ε in (4.19) and taking the limit $\delta/\varepsilon \ll 1$.

Remark 4.2. As mentioned, in case IIa, unlike in cases Ia or Ib, the second point $(u_+, p_R(u_+))$ at which ℓ^S and T_d intersect can also give rise to two-pulse orbits. We restrict attention to the triangle in the first quadrant of the c - σ plane bounded above by $c = -2\sigma + (1/6)$. From (4.10) and the definition of \tilde{H} , $u_+ = 6/(1 - \tilde{H})$, one finds $p_R(u_+) = \varepsilon[1 - (6\sigma/1 - \tilde{H})]$ and also $p_L(u_+) = p_R(u_+) - (6\varepsilon/u_+) = \varepsilon[\tilde{H} - (6\sigma/1 - \tilde{H})]$. Clearly, there is now a possibility to have $p_L < 0$. This condition is equivalent to $6(c + \sigma)^2 - c > 0$. Then, by direct calculation, one verifies that there is a subset of the triangle in which this condition holds, namely, it holds for all (c, σ) pairs with $1/24 \leq \sigma < 1/12$, and when $0 < \sigma < 1/24$ it holds for those (c, σ) pairs in which either $c > c_+$ or $c < c_-$, where $c_{\pm}(\sigma) = (1/12) - \sigma \pm (1/12)\sqrt{1 - 24\sigma}$.

Remark 4.3. The stability of the modulated two-pulse solutions in cases Ib and IIa can be studied exactly along the same lines as in section 4 of part I.

5. The self-replication process. We focus here on some questions and observations about various aspects of pulse splitting in which the slow variation of $U(x, t)$ plays a central role. The stability analysis in part I shows that there is a large domain in the parameter space in which both the stationary one-pulse patterns of section 2 (and [2]) and the slowly modulated two-pulse solutions are stable; see Figure 2. Part of the boundary of this domain is given by a line $A = \mathcal{O}(B^2)$, and it is precisely when this line $\mathcal{C}_{\text{SPLIT}}$ is crossed that the one-pulse patterns no longer exist (see section 6 of [3]) and that the self-replication process starts [3]; i.e., as ε is increased above this critical value, the stationary one-pulse solution splits into a pair of slowly modulated pulses. In particular, it can be shown that there is a critical value of ε , $\varepsilon_{\text{split}}$, so that for $\delta \ll 1$ there exists a stationary one-pulse homoclinic solution to (1.1) for all $\varepsilon < \varepsilon_{\text{split}}$. This result was obtained in section 6 of [3] using topological shooting arguments in a special choice for the parameters A, B , and D (see Remark 4.1). Since the scaled ODE (6.1) in [3] has the same essential structure as the ODE (1.5) here in so far as the topological shooting is concerned, a duplication of the arguments given in [3] shows that the stationary homoclinic one-pulse solution of (1.5) cannot exist for

$$\varepsilon > \varepsilon_{\text{split}} \quad \text{i.e., } A > \varepsilon_{\text{split}}^2 B^2.$$

In the terminology of [3], the solution “disappears,” and numerically, one observes the start of the self-replication process for $\varepsilon > \varepsilon_{\text{split}}$. This key role of the “disappearance” of the stationary one-pulse solution at the start of the self-replication process was already acknowledged in [19]; see section 6. This “disappearance bifurcation” was identified as a homoclinic saddle-node bifurcation in [16].

Furthermore, it was found in [19, 18, 2, 20, 3, 16, 14] that there are stable periodic multipulse patterns that appear as end products of the self-replicating process. These solutions were constructed in [2]: their structure in phase space is very similar to that of the homoclinic pattern: the solution is close to the slow manifold except for a homoclinic “jump” through the fast field (see Figure 2 in [2]).

These observations raise two questions: why do (some of) the periodic multipulse patterns still exist for $\varepsilon > \varepsilon_{\text{split}}$, and why does the pair of outward modulated pulses still exist for $\varepsilon > \varepsilon_{\text{split}}$ (as can be observed in numerical simulations)? After all, the construction of both of these types of solutions is based on the same asymptotic method that breaks down for the stationary one-pulse at $\varepsilon = \varepsilon_{\text{split}}$.

The formal answer to both these questions can be found by examining the magnitude and dynamics of $U(x, t)$ in the region where $V(x, t)$ has a pulse. For both of these types of solutions, the value of U in the pulse intervals is *significantly larger* than that of the stationary one-pulse. For the traveling pulses this can be seen, in terms of the scaling (1.3) $U(x, t) = (\delta/\varepsilon)u_-$ in a pulse interval (3.1), as follows: whereas one finds $u_- \approx 6$ at the initial stage of the splitting process (where c is near its maximum $1/6$), one sees that $u_- = 3$ for the stationary pulse ($c = 0$). Similarly, for the multipulse spatially periodic patterns, formula (2.9) in [3] shows that the value of u_- is much larger than that of the stationary one-pulse.

What is the importance of this fact that the U values are significantly larger and correspondingly that the amplitudes V are smaller (2.10)? Observe that in the (u, p) -equations of (1.5) $\ddot{u} = \varepsilon^2[uv^2 + \text{h.o.t.}]$, the term with v depends on u . As was done in part I, one can reexpress this u dependence (to leading order) by introducing \hat{v} : $v(\xi) = \hat{v}(\xi)/u$; where \hat{v} is now a solution of $\ddot{\hat{v}} = -\hat{v}^2 + \hat{v}$, that is independent of u to leading order. Hence, the leading order equation is

$$\ddot{u} = \frac{\varepsilon^2}{u}[\hat{v}^2 + \text{h.o.t.}],$$

and the leading order influence of u occurs through the factor ε^2/u , which may be labeled as an “effective” value of ε . This implies that those solutions having a higher value of u during the pulse interval are really solutions of a system that has a lower effective ε . Interpreting this for modulated two-pulse solutions, we see that they can exist in the regime where the actual ε is greater than $\varepsilon_{\text{split}}$ as long as the value of U is large enough so that the effective ε lies below $\varepsilon_{\text{split}}$. In this way, this solution can exist in a regime where the stationary one-pulse no longer does. A similar argument can be made for the multipulse solutions. This explains heuristically the existence of both the pairs of traveling pulse solutions and the singular periodic multipulse solutions, respectively, in the regime $\varepsilon > \varepsilon_{\text{split}}$, where the stationary one-pulse no longer exists.

The same heuristic extrapolations of the asymptotic analysis explain why two slowly modulated pulses traveling apart from each other split again after long enough time (on a large enough interval). Once again the value of U on intervals in which V has a pulse is the key to understanding this: $c(t)$ decreases monotonically to 0, and therefore, by (3.1), u_- decreases slowly from 6 to 3, the value of the stationary pulse. Thus, the “effective ε ” has increased to above $\varepsilon_{\text{split}}$. Moreover, for the modulated two-pulses this also yields a certain time T_{split} corresponding to when the effective value of ε crosses through $\varepsilon_{\text{split}}$ (i.e., the value of u_- becomes small enough), and both traveling pulses undergo splitting. The time T_{split} will depend on $\Delta\varepsilon = \varepsilon - \varepsilon_{\text{split}}$, and T_{split} decreases as $\Delta\varepsilon$ increases, as can be checked by numerical simulations. However, it should be noted that simulations of this mechanism are highly sensitive to boundary effects, and one must be sure to work on a sufficiently large domain.

The above arguments are far from rigorous. The most important obstacle is the fact that $\varepsilon_{\text{split}}$ is not an asymptotically small value. On the contrary, it is a well-defined $\mathcal{O}(1)$ number; see Table 1 in [3]. Thus, we cannot expect that “ u is constant to leading order” or that “ \hat{v} does not depend on u to leading order” in “the

fast field”: this terminology is applicable only when ε is asymptotically small and one can do a perturbation analysis. Nevertheless, the existence of an $\varepsilon_{\text{split}}$ value for slowly modulated two-pulse solutions can be made rigorous by employing the same topological shooting method as was established in [3] for the stationary one-pulse solutions. We do not consider this in any more detail in this paper.

In addition, we did not pay any attention to the “leading order” perturbations of $\mathcal{O}(\varepsilon^2)$ in the \hat{v} -equation, although one can argue on formal grounds that these “perturbations” do not give a net contribution.

On a bounded interval, the splitting process will come to a halt when the outward traveling pulses approach the boundary of the domain [19, 18, 2, 20, 3, 16, 14]. In Remark 6.1 the influence of having a bounded interval on the above described process, where it is implicitly assumed that $x \in \mathbf{R}$, is briefly discussed. The end product of the splitting dynamics is a periodic multi-pulse pattern that has a “large enough” value of U in the V -pulses. It has been checked in [3] that this multipulse pattern will also split as soon as ε is increased above a certain critical value, which depends monotonically on the wave length; see the discussion in section 6 and Table 3 in [3]. This is consistent with the heuristic arguments: the effective value of ε also increases when ε increases. See also Remark 5.1.

Finally, the reduction of the effective value of ε cannot be larger than $\mathcal{O}(1) \times \varepsilon$. Therefore, one cannot expect to see the traveling pulses for ε “far” from $\varepsilon_{\text{split}}$, i.e., for $\Delta\varepsilon$ “too large.” At first, it seems that this contradicts the numerical simulations in [19, 18, 2, 20, 16, 14]; however, a more careful study of these simulations reveals that there is no contradiction. On the contrary, these simulations are consistent with our arguments, since they indicate that the traveling pulses are no longer of the type studied in this paper when $\Delta\varepsilon$ becomes “too large.” Numerous figures in [19, 18, 2, 20, 16, 14] clearly show that, in this case, the speed c of the (most) outward traveling pulses *does not decrease* as a function of time between two successive splittings. Furthermore, these pulses are *not stationary* in a coordinate system traveling with speed c : the shape of the pulses changes as a function of time, especially at the trailing edges of the pulses; see Figure 4 here, Figure 9 in [2], Figure 2 in [20] and Figure 5.3 in [16]. Thus, these pulses are of an essentially different type. These simulations also strongly suggest that these traveling pulses can even be stable for certain parameter combinations: Figure 5.3 in [16] shows a solitary pulse traveling with constant speed with a periodic modulation of its trailing edge. Moreover, the distinction between a splitting process with pulses whose speeds slowly decrease to 0 for ε near $\varepsilon_{\text{split}}$ and a splitting process with pulses whose speeds are constant for ε not near $\varepsilon_{\text{split}}$ is of course not exact: numerical simulations also show that there is a transition region where the speed of the pulses first decreases slowly, but after some time (on the slow time scale), the speed remains constant, > 0 . The existence analysis for these intriguing constant speed solutions asks for an approach that differs essentially from that in this paper, since these solutions appear from numerical simulations to exist only in regions where the existing asymptotic methods are not applicable. On the other hand, some perturbation analysis may be possible, since the shape of the pulses certainly is singular, and the modulations seem to evolve slowly (section 6).

Remark 5.1. Even for $\varepsilon \gg \varepsilon_{\text{split}}$ there can still be spatially periodic multipulse patterns. Heuristically, for ε large but not too large, this follows from the fact that the maximum value of U in a pulse interval increases monotonically (without bound) as the wave length decreases [2, 3]; i.e., the effective value of ε can “always” be reduced below $\varepsilon_{\text{split}}$. Once ε becomes too large, however, then this heuristic “scheme” is no

longer applicable, since the V -pulses lose their singular structure and the wave length of the periodic patterns becomes smaller and smaller as ε increases (see Figure 10 in [2] and see [13]).

This regime is studied in detail in [13], where it is shown that eventually the periodic solutions no longer “touch down” on the slow manifold (in the phase space), and they become nonsingular periodic orbits. Moreover, it is shown there that these orbits are finally annihilated in a Turing/Ginzburg–Landau bifurcation in the PDE (which is manifested in the associated ODE as a reversible 1 : 1 resonant Hopf bifurcation).

Remark 5.2. The above explanation of why traveling pulses will split only after a certain (long) time is a reformulation into geometrical terms of subsection 3.4 of part I: “perturbations” that can be assumed to be small enough immediately after the first splitting will grow slowly as time evolves.

Remark 5.3. In order to present a detailed description of the dynamics during splitting events, one needs a method to study “fully interacting” pulses, which is stronger than that used to study “mildly strong interacting” pulses in this work (where it is always assumed that the V -pulses of the modulated two-pulse solutions are separated). This is because the splitting process itself is a relatively fast one (see, for instance, [16] and Figure 6 in [2]), and hence the quasi-stationary approach developed here is no longer applicable. So far, a detailed quantitative description of the behavior of (U, V) for fully interacting pulses does not yet exist.

6. A discussion of the literature. The paper by Reynolds, Ponce-Dawson, and Pearson [19] was the first paper in which this process was studied as an important and interesting general phenomenon (earlier examples of the self-replication process certainly exist; see the references in [19]). Reynolds, Ponce-Dawson, and Pearson present an explanation for the self-replication process in the Gray–Scott model. The analysis in this paper, and its follow-up [20], is a mixture of numerical simulations and formal asymptotic methods, in which $\delta^2 = D$ (in this paper) is the only small parameter, i.e., A and B are considered as $\mathcal{O}(1)$ parameters (thus, the richness of scalings in the Gray–Scott model, as we deduced in part I of this work, was not recognized in [19, 20]).

The main result of [19, 20] is the computation of a relation between the speed c of a pulse and the “fluxes” L^\pm into the pulse. These fluxes are computed from the equations that describe the “outer expansions.” These equations are in essence identical, modulo scalings, to the leading order part of the equations that describe the slow flow on \mathcal{M} (2.1), in case Ia, the most generic case (1.6). As a consequence, the quantity $c(L^+, L^-)$ in [19, 20] corresponds directly to our results in subsection 3.1, where we express c in terms of $\hat{\xi}_{\max}$ (3.5) and u_{\max} (3.6), or vice versa (L^\pm can be expressed in terms of $\hat{\xi}_{\max}$ and u_{\max}). In our case, the expressions are completely explicit, while they follow from numerical computations in [19, 20]. This is because in this work, the fast system can be reduced by the scalings (1.3) to an integrable ODE (2.9), while the corresponding “inner expansion” in [19, 20] is a full four-dimensional ODE that has to be solved numerically (see [20] for details). For the same reason, the evolution of c as function of t , as is done here in subsection 3.2 and in section 4, cannot be done analytically in [19, 20].

On the other hand, the “disappearance” of the stationary one-pulse solution has been identified in the plots of $c(L^+, L^-)$ in [19, 20] (recall that $A = B = \mathcal{O}(1)$ in [19, 20], thus $\varepsilon = \mathcal{O}(1)$ (1.4)). The crucial role of this “disappearance” for the start of the self-replication process has been mentioned in [19] for the first time in the literature. Moreover, the numerical/asymptotical methods of [19, 20] can be, and have

been, applied to the domain $\varepsilon = \mathcal{O}(1)$, where the asymptotic methods developed in this work need to be replaced by the topological shooting arguments first developed in [3]. Thus, the evolution of the modulated pulses with constant (nondecreasing) speed mentioned above, can be discussed in terms of this approach, as is done in [20]. There, it is argued that the self-replication process for these pulses is also related to changes in the stability of the pulses (in [19, 20] the linearized stability of the pulses is determined numerically). If the argument there holds, then the self-replication mechanism suggested in [20] differs essentially from that of the stationary one-pulse solution, and that of the slowly modulated two-pulse solution with nonconstant speed as discussed in section 5, since the start of the replication process in these cases can be explained in terms of a “disappearance (= homoclinic saddle-node [16]) bifurcation.” Apparently, the “dynamical” self-replications of slowly modulated two-pulse solutions with decreasing speed studied in this work is not discussed in [19, 20].

In [16] a “skeleton structure” that is postulated to be the “backbone” of the self-replication process is described, based on numerical evidence in the Gray–Scott model and another model problem. The presence of a hierarchy of saddle-node points (i.e., “disappearance bifurcations”) lies at the heart of this structure, both for the pulses with constant speed and those with slowly decreasing speed. This “skeleton structure” mechanism has a number of essential similarities with the mechanism described in [2, 3] and this work, as we shall discuss below. Hence, at this moment there exist two different explanations for the self-replication process of traveling pulses with constant speed. As already noted in the previous subsection, this is also the case for which an analytical treatment is still nonexistent.

On a bounded domain, the hierarchy described in [16] consists of a family of saddle-node bifurcations of the 1, 2, 3, . . . -pulse patterns at “almost the same” value of a bifurcation parameter, say, the ε used in this paper. This “hierarchy” corresponds to and agrees with the analysis and observations in [2, 3]. There, the N -pulse patterns ($N > 1$) on a bounded domain are identified as elements of a (continuous) family of stationary, spatially periodic, solutions that approach the homoclinic one-pulse pattern, in the four-dimensional phase space, as the period \mathcal{T} goes to ∞ . Although the analytical details of the splitting of these periodic solutions have not been worked out in [3], their closeness to the homoclinic orbit (in the phase space) immediately implies that a \mathcal{T} -periodic orbit will split at a value $\varepsilon_{\text{split}}(\mathcal{T})$ with $\lim_{\mathcal{T} \rightarrow \infty} \varepsilon_{\text{split}}(\mathcal{T}) = \varepsilon_{\text{split}}$, the critical value of the (limiting) homoclinic orbit. Thus, if the length L of the interval is “long enough,” the period \mathcal{T} of the periodic N -pulse patterns, i.e., the distance between successive pulses, $\mathcal{T} = L/N$, will be “large” if N is “not too large” (we refer to [3] for an explicit asymptotic expression for \mathcal{T} in terms of the parameters in the Gray–Scott model (in the scaling given in Remark 4.1); this expression can be used to quantify the statements “long enough,” “large,” etc.). As a consequence, these pulses will split at the value $\varepsilon_{\text{split}}(\mathcal{T})$ of the bifurcation parameter ε that is very close to $\varepsilon_{\text{split}}$ of the homoclinic one-pulse pattern. This is confirmed by the numerical simulations in [3] (see Table 3). Hence, the analysis in [2, 3] confirms the existence of the “hierarchy of saddle-node bifurcations” described in [16] (on domains that are “long enough”). Moreover, the dynamics of the modulated two-pulse solutions as described in this work can be interpreted as giving an analytical description of the evolution of the pulse solutions that have already split in between two successive steps of the hierarchy described in [16], or at the end of this process (see also Remarks 3.5 and 6.1).

The first steps into the direction of a rigorous theory for this “skeleton structure

of saddle-node bifurcations” and the type of splitting dynamics it implies are taken in [7]. This approach is based on a number of assumptions on the existence and stability properties of the pulse patterns that have not yet been validated. The analysis in this paper, in combination with that in [2, 3], could be used as a foundation for such a validation in the case of the slowly modulated two-pulse solutions with slowly decreasing speed. See also [5].

Remark 6.1. In the heuristic explanation of the dynamical splitting process of section 5, it is implicitly assumed that it takes place on an unbounded domain, so that a pair of pulses that have split can eventually be considered as the superposition of two (almost) stationary homoclinic one-pulse patterns (at leading order) that will split as soon as the “effective” value of ε has increased above $\varepsilon_{\text{split}} = \varepsilon_{\text{split}}(\infty)$. In the case of a bounded interval of length L , the same arguments can be applied, but now the role of the superposition of two (almost) stationary homoclinic one-pulse patterns must be taken over by a spatially periodic two-pulse solution. This implies that the critical value of the “effective” ε is not equal to $\varepsilon_{\text{split}}$ but to $\varepsilon_{\text{split}}(L/2) > \varepsilon_{\text{split}} = \varepsilon_{\text{split}}(\infty)$ [3].

REFERENCES

- [1] A. DOELMAN, W. ECKHAUS, AND T.J. KAPER, *Slowly modulated two-pulse solutions in the Gray–Scott model I: Asymptotic construction and stability*, SIAM J. Appl. Math., 61 (2000), pp. 1080–1102.
- [2] A. DOELMAN, T.J. KAPER, AND P. ZEGELING, *Pattern formation in the one-dimensional Gray–Scott model*, Nonlinearity, 10 (1997), pp. 523–563.
- [3] A. DOELMAN, R.A. GARDNER, AND T.J. KAPER, *Stability analysis of singular patterns in the 1-D Gray–Scott model: A matched asymptotics approach*, Phys. D, 122 (1998), pp. 1–36.
- [4] A. DOELMAN, R.A. GARDNER, AND T.J. KAPER, *Large stable pulse solutions in reaction-diffusion equations*, Indiana Univ. Math. J., 49 (2000).
- [5] A. DOELMAN AND T.J. KAPER, *Pulse dynamics in singularly perturbed reaction-diffusion systems*, in preparation.
- [6] W. ECKHAUS, *Asymptotic Analysis of Singular Perturbations*, North-Holland, Amsterdam, 1979.
- [7] S. EI, Y. NISHIURA, AND B. SANDSTEDT, *Pulse-interaction approach to self-replicating dynamics in reaction-diffusion systems*, in preparation.
- [8] N. FENICHEL, *Geometrical singular perturbation theory for ordinary differential equations*, J. Differential Equations, 31 (1979), pp. 53–98.
- [9] P. GRAY AND S.K. SCOTT, *Autocatalytic reactions in the isothermal, continuous stirred tank reactor: oscillations and instabilities in the system $A + 2B \rightarrow 3B$, $B \rightarrow C$* , Chem. Engrg. Sci., 39 (1984), pp. 1087–1097.
- [10] J.K. HALE, L.A. PELETIER, AND W.C. TROY, *Exact homoclinic and heteroclinic solutions of the Gray–Scott model for autocatalysis*, SIAM J. Appl. Math., 61 (2000), pp. 102–130.
- [11] G.M. HEK, *Fronts and pulses in a class of reaction-diffusion equations: A geometric singular perturbations approach*, Nonlinearity, 14 (2001), pp. 35–72.
- [12] C.K.R.T. JONES, *Geometric singular perturbation theory*, in Dynamical Systems, Montecatini Terme, 1994, Lecture Notes in Math. 1609, R. Johnson, ed., Springer, Berlin, 1995, pp. 44–118.
- [13] D.S. MORGAN, A. DOELMAN, AND T.J. KAPER, *Stationary periodic orbits in the 1-D Gray–Scott model*, Methods Appl. Anal., 7 (2000), pp. 105–150.
- [14] C. MURATOV AND V. OSIPOV, *Spike Autosolitons in the Gray–Scott Model*, preprint.
- [15] W.-M. NI, *Diffusion, cross-diffusion, and their spike-layer steady states*, Notices Amer. Math. Soc., 45 (1998), pp. 9–18.
- [16] Y. NISHIURA AND D. UEYAMA, *A skeleton structure for self-replication dynamics*, Phys. D, 130 (1999), pp. 73–104.
- [17] J.E. PEARSON, *Complex patterns in a simple system*, Science, 261 (1993), pp. 189–192.
- [18] V. PETROV, S.K. SCOTT, AND K. SHOWALTER, *Excitability, wave reflection, and wave splitting in a cubic autocatalysis reaction-diffusion system*, Phil. Trans. Roy. Soc. London Ser. A, 347 (1994), pp. 631–642.

- [19] W.N. REYNOLDS, J.E. PEARSON, AND S. PONCE-DAWSON, *Dynamics of self-replicating patterns in reaction diffusion systems*, Phys. Rev. Lett., 72 (1994), pp. 2797–2800.
- [20] W.N. REYNOLDS, S. PONCE-DAWSON, AND J.E. PEARSON, *Self-replicating spots in reaction-diffusion systems*, Phys. Rev. E, 56 (1997), pp. 185–198.
- [21] C. ROBINSON, *Sustained resonance for a nonlinear system with slowly varying coefficients*, SIAM J. Math. Anal., 14 (1983), pp. 847–860.